HOUSING SHAPE'S IMPACT ON ELECTRIC SUBMERSIBLE PUMP'S EQUILIBRIUM POSITION AND ROTORDYNAMICS

A Thesis

by

CLAY SVEN NORRBIN

Submitted to the Office of Graduate and Professional Studies of
Texas A&M University
in partial fulfillment of the requirements for the degree of

MASTER OF SCIENCE

Chair of Committee,	Dara W. Childs
Committee Members,	Gerald Morrison
	Thomas A. Blasingame
Head of Department,	Andreas A. Polycarpou

December 2016

Major Subject: Mechanical Engineering

Copyright 2016 Clay Sven Norrbin

ABSTRACT

Electric Submersible Pumps (ESPs) are a subgroup of pumps designed to have small diameters to accommodate tight working environments. The long length of an ESP (5-100 stages) requires a large amount of annular seals. Each seal provides a lateral reaction force for the rotor. Lateral loading caused by gravity and housing curvature changes the running position of the rotor in these seals. The running position of the rotor with respect to the housing is the Static Equilibrium Position (SEP). The SEP is important in determining the rotordynamic coefficients for the bearings/seals. An SEP analysis suitable for ESPs is shown. The analysis predicts the equilibrium position due to gravity and/or curvature loading in the well casing as well as for surface applications. The analysis can accept seals with eccentricity-dependent reaction forces. The code also interfaces with response codes to predict the rotordynamic characteristics of motion around the equilibrium position. The rotor or housing can be set to any prescribed position, and the remaining stations can be solved for.

A static and rotordynamic analysis is presented for an ESP model. This model is of a Baker Hughes G400 ESP pump. This study first finds the SEP and then shows a rotordynamic analysis about the SEP. Predictions are shown in a horizontal and a vertical orientation. In these two configurations viscosities and clearances are varied through 4 cases of: (1) Viscosity of 1 cP and interstage seal clearances of 127 μm (2) Viscosity of 1 cP and interstage seal clearances of 381 μm (3) Viscosity of 30 cP and interstage seal

clearances of 127 μm (4) Viscosity of 30 cP and interstage seal clearances of 381 μm. The appropriate shorthand notations are: 1X 1cP, 3X 1cP, 1X 30cP, and 3X 30cP respectively.

In a horizontal, straight-housing position, the model includes gravity and buoyancy on the shaft. At 1X 1cP, the horizontal statics show a moderate eccentricity ratio of 0.53 for the shaft with respect to the housing. With 3X 1cP, the static eccentricity ratio is increased to 0.76. With 1X 30cP, the predicted static eccentricity ratio is low at 0.08. Increasing the clearance to 3X 30cP, the predicted eccentricity ratio increases to 0.33. No horizontal case is expected to rub. With the housing is supported at five different housing positions instead of fixed straight, the static position had relatively no change.

Predictions for a vertical case of the same model are also presented. The curvature of the housing is varied until rub or close-to-wall rub is expected. The curvature needed for a rub with a 1cP-1X fluid is 7.5 Degrees of Curvature (DOC). The DOC is a metric for curvature. It is defined as the amount of degrees which pass around a constant curve of 33.3 m in length. The stability of the system with changing curvature is presented, and curvature is shown to have a minor impact. With 3X 1cP, there is a decrease in maximum eccentricity, but with more seals loaded than with 1X 1cP. With 1X 30cP, a smaller length of shaft that deviates from the housing centerline's position. The maximum curvature for a static rub with 1X 30cP is greater than 25 DOC. Both 1X 30cP and 3X 30cP are unstable. No dynamic data predictions are shown for 30 cP since the model is unstable. The static position for 3d housing shape with 1 cP fluid is lastly presented. A helix as the housing shape is used due to constant curvature. With respect to a curvature in only the *Y* direction, the helix static shape differed from the *Y*-*Z* plane curvature in attitude angle.

ACKNOWLEDGMENTS

Thank you Dr. Dara Childs for providing excellent guidance throughout this project. Your passion pushes all of your students to the best of their abilities. You will be greatly missed once you depart. I am honored to be one of your last students. I would also like to thank my Mother, Father, and Sister for always being there to talk and to keep me working hard. I am always proud of having such a smart, motivated, and loving family. I would like to thank my Grandfather and Moms who both have always been there for support and motivation.

Thank you to all of those who have helped make my time here memorable: Matt, Jesse, Mauricio, Jose, Andrew, Jen, David, Jimmy, Josh, Travis, Nathan, and Keith. Our time together will always be remembered.

NOMENCLATURE

a_{maj}	Major dynamic distance from SEP to Rotor's center [L]
a_{min}	Major dynamic distance from SEP to Rotor's center [L]
C_{ij}	Damping Coefficient [FT/L]
C_r	Radial clearance [L]
$[C_1]$	Matrix that is constant through Newton-Raphson [-]
$[C_2]$	Matrix that is constant through Newton-Raphson [-]
D	Diameter of Seal [L]
D_A	Arc Length Degree of Curvature [Angle]
e_X	Distance in X direction from Bearing/Seal center to SEP [L]
e_Y	Distance in Y direction from Bearing/Seal center to SEP [L]
e_0	Distance from the Bearing/Seal center to SEP [L]
F_i	Dynamic Force in X and Y directions [F]
$\{F\}$	Static force vector [F]
$\{G\}$	Newton-Raphson error vector [F]
$[J]$	Jacobian of Newton-Raphson error vector [-]
K	Stiffness Coefficient [F/L]
$[K]$	Stiffness matrix [F/L]
$[K_T]$	[K] for non-eccentricity-dependent stations [F/L]
$[K_U]$	[K] for linear coordinates and non-linear forces [F/L]
$[K_V]$	[K] for non-linear coordinates and linear forces [F/L]

$[K_W]$	[K] for non-linear coordinates and non-linear forces [F/L]
L	Length of Seal [L]
L_{arc}	Arc length for the Degree of Curvature [L]
M_{ij}	Virtual mass coefficient [M]
R_c	Radius of Curvature [L]
U_{TX}	Dynamic displacement about SEP in X direction [L]
U_{TY}	Dynamic displacement about SEP in Y direction [L]
$\{U\}$	Steady State Displacement vector [L]

Greek

ζ	Damping Ratio [--]
ϵ_0	Eccentricity Ratio (e_0/C_r) [--]
$\boldsymbol{\lambda}$	Complex eigenvalues [T^{-1}]
ω_n	Natural Frequency [T^{-1}]
ω_d	Damped Natural Frequency [T^{-1}]
ϕ	Attitude angle: Angle between load and eccentricity [Angle]
ψ	Angle between dynamic motion ellipse and X Axis [Angle]
δX	Dynamic displacement in X direction [L]
δX	Dynamic displacement in X direction [L]
ΔX	Relative rotor-housing displacement in X direction [L]
ΔY	Relative rotor-housing displacement in Y direction [L]

Subscripts

eq	Equilibrium position
i	Direction of response, either X or Y
j	Direction of response, either X or Y
L	Linear forces or displacements
n	Iteration number
NL	Non-linear forces of displacements
RMS	Root Mean Squared
MAX	Maximum value of vector

Abbreviations

DOC	Degree of Curvature. Defined in 1.1
ESP	Electric Submersible Pump
FEM	Finite Element Model
PSR	Pre-swirl Ratio. Defined in 2.1
SEP	Static Equilibrium Position. Defined in 1.3

TABLE OF CONTENTS

Page

ABSTRACT ii

ACKNOWLEDGMENTS iv

NOMENCLATURE v

TABLE OF CONTENTS viii

LIST OF FIGURES x

LIST OF TABLES xiii

1. INTRODUCTION 1

1.1 Electric Submersible Pump Background 1
1.2 Rotordynamics of ESP Pump Section Background 13
1.3 Static Equilibrium Position Background 15

2. STATEMENT OF WORK 20

3. METHOD 21

3.1 Statics Derivation 21
3.2 Setting Curvature of the Housing Derivation 23
3.3 Code Outline 24

4. CODE VALIDATION 27

4.1 Gravity Loading on Multiple Eccentricity-Dependent Seals 27
4.2 Uniform Curvature Multi-Seal Model 32

5. PREDICITIONS FOR SAMPLE ESP 37

5.1 ESP Pump Section Model 37
5.2 Statics of a Horizontal ESP 41
5.3 Intermediate Support Horizontal Statics 44
5.4 Statics of Vertical Mounted ESP with Housing Curvature 45
5.5 Dynamic Stability about Equilibrium Position 54
5.6 Dynamics around Equilibrium Position 56
5.7 Equilibrium Position of Vertical ESP with Helical Housing Position 62

6. CONCLUSION 65

6.1 Predictions for Horizontal ESP 65
6.2 Predictions for a Vertical ESP with Imposed Curvature 66
6.3 Static Predictions with a Vertical 3-D Curve Profile 67
6.4 Future Work 67

REFERENCES 69

APPENDIX A. STATICS DERIVATION 72

APPENDIX B. GRAVITY DERIVATION 79

APPENDIX C. SEAL DATA FOR CODE VALIDATION 81

APPENDIX D. SEAL DATA FOR SAMPLE ESP PUMP 83

APPENDIX E. MAX DISPLACEMENT GRAPHS 85

LIST OF FIGURES

Page

Figure 1.1: Component view of an ESP. The ESP is not limited to this height. It may sit several thousand feet from the controller. [2].....2

Figure 1.2: Example of well paths for oil well. ESP will sit near well at a minimum depth to avoid loss of suction. [3] 3

Figure 1.3: Degree of Curvature (DOC) relation to the curvature of a circle 4

Figure 1.4: ESP in curving well casing. Light blue is the ESP string. The red-yellow-green tubing is the well casing [5] 5

Figure 1.5: ESP in a surface mounted installation. Intermediate supports are used to hold housing in place. [6].....6

Figure 1.6: View of ESP sections showing which section this thesis covers. [1].....8

Figure 1.7: Radial vs. mixed flow impellers. [9].....9

Figure 1.8: Example of mixed flow impeller. Seals are listed in red. 11

Figure 1.9: [13] ESP, tested by Forsberg, with accelerometers distributed along the housing to measure acceleration and response.....14

Figure 1.10: Rotor orbit around an SEP at one axial position.....16

Figure 1.11: Holmes model to show the affects of bearing misalignment. Shaft A and shaft B are rigidly connected. [17] 17

Figure 1.12: Model Gajan's Thesis used for verification of analysis. Center two bearings are the test bearings and were given lateral offsets. [19].....18

Figure3.1: Flow chart for static equilibrium position analysis.....26

Figure 4.1: Model for proving distributed loading. Gravity is acting in the negative *Y* direction. 28

Figure 4.2: Forces including gravity and seal reaction vs. Axial Position.....30

Figure 4.3: Displacement of the Rotor for Validation model 1. Load is in the –*Y* direction.....31

Figure 4.4: Convergence graph for validation model 1. G is the force vector at the seals. 32

Figure 4.5: Basic two line model to show the affects from curvature. 33

Figure 4.6: Applied force onto rotor from a constant curvature. This force profile is with cross coupled stiffness. 34

Figure 4.7: Static equilibrium position of basic curvature. Solution is the same with and without cross coupled stiffness. 35

Figure 4.8: Calculated relative rotor-housing eccentricities due to an imposed housing curvature on a rotor with linear seals. 36

Figure 5.1: Side view for 5 stages of Sample ESP model 37

Figure 5.2: Full model of ESP in XLTRC. All blue lines are seal locations. 38

Figure 5.3: 1 cP Horizontal static position with the housing fixed at zero displacement and standard gravity. 42

Figure 5.4: 30 cP Horizontal static position with the housing fixed at zero displacement and standard gravity. 43

Figure 5.5: Horizontally mounted ESP with intermediate support every 1.04 meters. Model is 1X 1cP 45

Figure 5.6: Profile of imposed curve on housing. 46

Figure 5.7: Three dimensional views of static equilibrium position in sample ESP pump section with 1X 1 cP. 47

Figure 5.8: Error graph for vertical 1 cP 1X Cr. G is the vector that Newton-Raphson solves for zero. RMS is Root Mean Sum of the vector. 48

Figure 5.9: SEP from curvature in the *Y-Z* plane on vertically mounted ESP. Case 1X 1cP. 49

Figure 5.10: SEP from curvature in the *Y-Z* plane on vertically mounted ESP. Case 3X 1cP. 51

Figure 5.11: SEP from curvature in the *Y-Z* plane on vertically mounted ESP. Case 1X 30 cP. 52

Figure 5.12: SEP from curvature in *Y-Z* plane on vertically mounted ESP. Case 3X 30 cP. 53

Figure 5.13: Damping ratio of sample 20 stage ESP with changes to curvature. Case 1X 30cP $\boldsymbol{\omega}$=3600 rpm 55

Figure 5.14: Damping ratio of sample 20 stage ESP with changes to curvature. Case 1X 1cP $\boldsymbol{\omega}$=3600 rpm 0.7 preswirl 56

Figure 5.15: Total relative response comparison between (A) 0 eccentricity and (B) Horizontal ESP predicted about equilibrium position.. 58

Figure 5.16: Total relative response comparison between (A) 0 eccentricity and (B) Horizontal ESP predicted equilibrium position. 59

Figure 5.17: Total relative response comparison between 4 different curvatures. All at 1X clearances and 1 cP as the process fluid. 60

Figure 5.18: Total relative response comparison between 4 different curvatures. All at 3X clearances and 1 cP as the process fluid. 61

Figure 5.19: Helical housing curvature versus a *Y-Z* housing curvature. 63

Figure 5.20: ESP with a two plane helix shape. 1 DOC and the ESP is 1X 1 cP. 64

Figure A.1: Multi-line model with rotors and housings 72

Figure A.2: Coordinate system for each node on the rotor or housing. 73

Figure B.3: Finite Element with uniform loading between nodes 79

Figure D.4: Force vs. Eccentricity for seals used on 20 stage example. 1X 1cP 83

Figure D.5: Force vs. Eccentricity for seals used on 20 stage example. 3X 1cP 83

Figure D.6: Force vs. Eccentricity for seals used on 20 stage example. 1X 30cP 84

Figure D.7: Force vs. Eccentricity for seals used on 20 stage example. 3X 30cP 84

Figure E.8: Static + dynamic maximum displacement vs. axial distance for a 1X 1cP case. 85

Figure E.9: Static + dynamic maximum displacement vs. axial distance for a 3X 1cP case. 86

LIST OF TABLES

Page

Table 4.1: Seal Properties for single line validation model. Running speed of 3600rpm 28

Table 4.2: Stiffness with respect to eccentricity for validation model. Running speed of 3600rpm. 28

Table 4.3: Seal stiffness coefficients for multi-seal supported rotor. 33

Table 5.1: Seal geometry for a single ESP stage 39

Table 5.2: Different seal configurations for sample ESP pump 40

Table 5.3: PSR, eq. (4.1), for seals in model. 40

Table C.1: Stiffness with respect to eccentricity for validation model. Running speed of 3600rpm. 81

Table C.2: Damping with respect to eccentricity for validation model. Running speed of 3600rpm. 81

Table C.3: Virtual mass with respect to eccentricity for validation model. Running speed of 3600rpm. 81

Table C.4: Force with respect to eccentricity for validation model. Running speed of 3600rpm. 82

1. INTRODUCTION

1.1 Electric Submersible Pump Background

Electrical Submersible Pumps (ESPs) represent a subgroup of pumps with enclosed motor units that can withstand contamination from the production fluid. This allows the motor to be directly attached to the pump and the whole unit to be submerged in the production fluid. ESPs come in a large variety of sizes. This thesis is focused on long multistage ESPs. These ESPs are commonly used in oil recovery. If an oil well does not have sufficient pressure to maintain an economical flow, artificial lift methods are used to extract the oil. There are two types of pumps used for artificial lift: positive displacement pumps and dynamic displacement pumps. ESPs are the most commonly used dynamic displacement pump [1]. ESPs are the best choice for large flow recovery of low Gas Volume Fraction (GVF) oil wells. Figure 1.1 shows the typical sections of an ESP. An ESP typically has 4 main sections: (1) A sensor, (2) a motor, (3) a seal chamber, and (4) a pump section. Some ESPs may include a gas separator before the ESP pump section if the well has a high GVF.

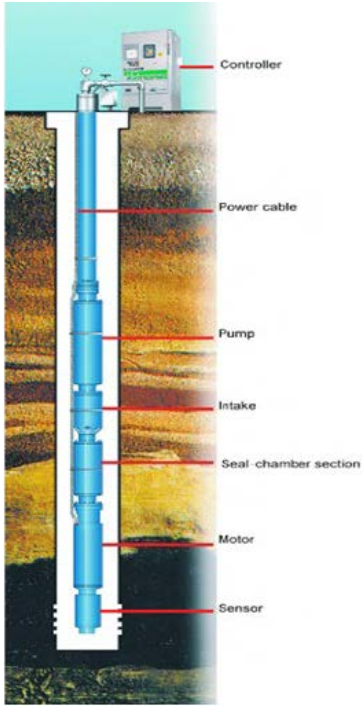

Figure 1.1: Component view of an ESP. The ESP is not limited to this height. It may sit several thousand feet from the controller. [2]

ESPs can be operated in either a caisson on the mud line or in the well casing. The well casing is the constructed barrier to keep the integrity of the drilled hole. The decision to place an ESP at the mud line or in the well casing depends on the wells conditions, this includes the depth of the well and the well's natural production rate. The reason for putting an ESP in the well casing is the ESP must have adequate suction pressure for efficient operation.

A well casing generally does not have zero curvature. The well path can deviate away from a straight line for many different reasons, including: avoiding rock formations, avoiding past drilled paths, avoiding broken drill bits, etc. Figure 1.2 is an example of the different paths a well casing might take. The figure is used for example purposes only, it is not an accurate representation of the path a subsea ESP may operate. Each line is a

different drill path. ESPs have a certain depth they must sit. ESPs also may not fit all the way down the reservoir. This creates a region along the well casing where an ESP may operate. This region has a chance of having curvature along the ESP.

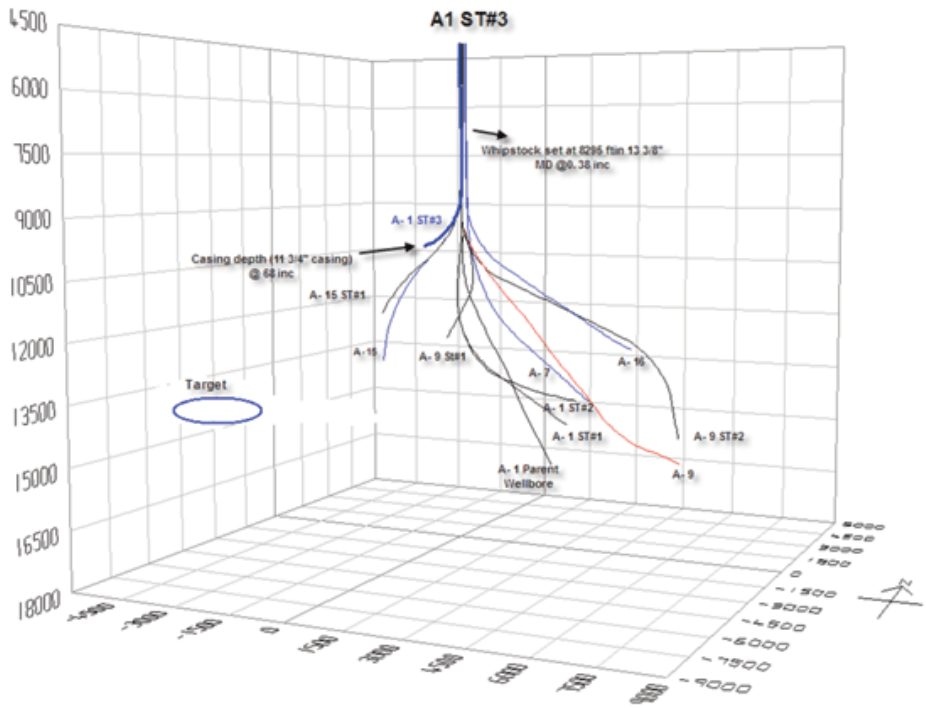

Figure 1.2: Example of well paths for oil well. ESP sits near well at a minimum depth to avoid loss of suction. [3]

The curvature of a well is typically measured using the arc length definition of Degree of Curvature (DOC). DOC is used for large radius of curvatures. There is an arc-length and a chord-length definition of DOC. Since the chord length method is more generally used, it will be used for this thesis. Figure 1.3 shows the relation between DOC and the radius of curvature (R_C). The maximum curvature is typically held below 5 DOC. The radius of curvature can be found from the degrees of curvature using

$$R_c = \frac{L_{arc} * 180}{DOC * \pi} \tag{1.1}$$

where R_c is the radius of curvature, L_{arc} is the arc length, and DOC is the degree of curvature. 33.3 *m* for an arc length is most commonly used in the oil industry so it will be used for the DOC in this study. No study exists that shows what curvature does to an ESP's rotordynamics. A code exists to determine the contact points and stresses imposed on the ESP, one is developed by CFER [4]. The seals in an ESP have a maximum reaction force before a rub occurs. No study exists that determines the maximum curvature that an ESP can handle before rubbing during operation.

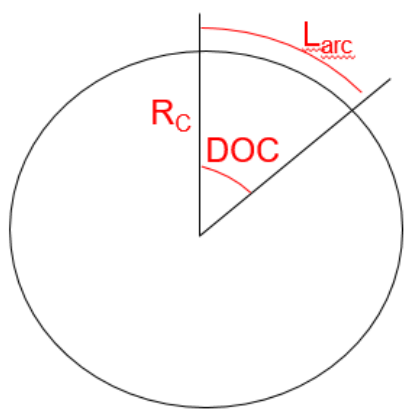

Figure 1.3: Degree of Curvature (DOC) relation to the curvature of a circle

An ESP will approximately follow the path of the well casing. Figure 1.4 shows an ESP in a 3D curved well casing. The radial gap between the ESP outer diameter and the well casing inner diameter is the housing-casing cavity. The annular clearance of the housing-casing cavity may vary. For this thesis, the housing-casing cavity is assumed to be 17.8 mm (0.7 in).

In designing an ESP to sit in a well the correct contact points between the ESP housing and well casing should be known. The contact points depend on the stiffness of the housing and rotor of the ESP as well as the curvature of the well casing. For this thesis, due to limited data, the specified curvature will be of the ESP housing itself and not the well casing.

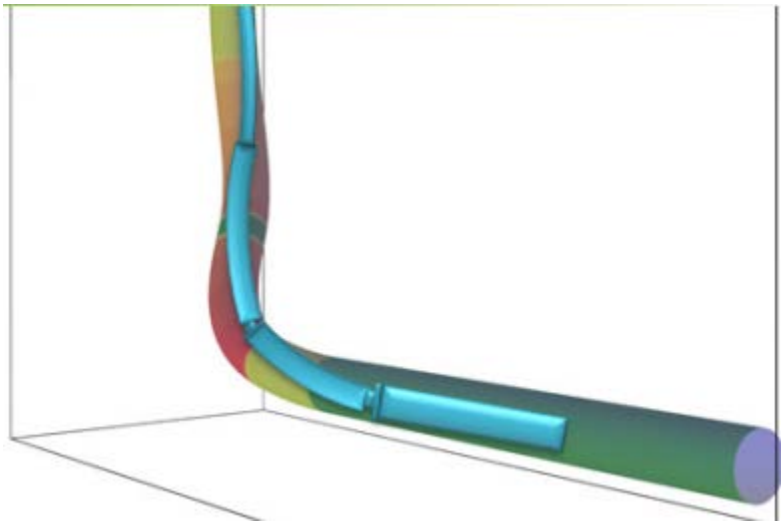

Figure 1.4: ESP in curving well casing. Light blue is the ESP string. The red-yellow-green tubing is the well casing [5]

A well casing may also lie in a horizontal configuration. An ESP in this circumstance will lie on the floor of the well casing. The housing is supported along the length of the pump for this configuration. The ESP rotor then has gravity acting laterally along the shaft.

It is also common for the pump section of an ESP to be in a surface mounted operation. Figure 1.5 shows an ESP for a surface mounted application. The ESP pump housing is the blue cylinder. There are intermediate supports holding the pump section to

an I-beam for support. For these applications, the ESP pump section is directly connected to a motor through a coupling. The model for a surface mounted ESP is similar to an ESP mounted in a horizontal well casing. The difference is that the surface-mounted operation has fixed positions for the housing at the intermediate supports, while the horizontal well casing model has the housing's position fixed at zero for its length.

Figure 1.5: ESP in a surface mounted installation. Intermediate supports are used to hold housing in place. [6]

To increase the economy of oil wells, there has been a recent push to improve ESP's reliability. Pflueger [7] predicts the current mean time to failure for a downhole ESP is between 500 days and 1000 days. End-users would like this number to improve to have more economical production. This increase in interest from end-users is increasing focus to the difficulties in modeling an ESP's rotordynamics. One important aspect of the rotordynamics is the Static Equilibrium Position (SEP) of the rotor. For most rotordynamics, linear analysis is adequate, and is performed for small motion about an equilibrium running position. Therefore, an adequate rotordynamic model to increase reliability in pumps needs an accurate SEP feature.

ESPs can be in a wide range of conditions for housing position. Two cases that are of particular interest are a horizontally-mounted housing and a vertical curved housing. Both of these cases are very distinct problems in rotordynamics. They cause changes to the SEP that can lead to rub or changes to the linear rotordynamics. This thesis aims to fill the gap in SEP rotordynamic codes by adding the ability to correctly calculate the SEP for ESPs.

In 1990, Durham [8] examined 100 ESPs' failure modes and determined that high vibration in the pump section of an ESP was the leading cause of failure. Durham's pumps were operating in a horizontal surface application. The ESPs had frequent motor-bearing and seal-chamber failures. He found that a majority of pump operators are not accurately classifying their failure mode. Durham stated that the highest vibration is coming from the pump section. The large vibration in the pump section then causes the seal-chamber section to prematurely wear causing failures to the motor. Durham also identifies the large vibration in the pumps as well past acceptable limits.

Due to the significant vibration of the pump section, this thesis only considers the pump section. Figure 1.6 shows an enlarged view of the pump section of an ESP. To allow for a smaller diameter, ESPs have many stages to adequately meet the head requirement. The typical diameter of ESPs range from 7.6 cm to 25 cm pump outer diameter. The smaller diameter allows ESPs to fit in tight well bores. These pumps can be from 3 to 40 meters long with 5 to 100 stages. The long length and small diameter make the shaft flexible with respect to conventional pumps. The same pump section is used for the surface application.

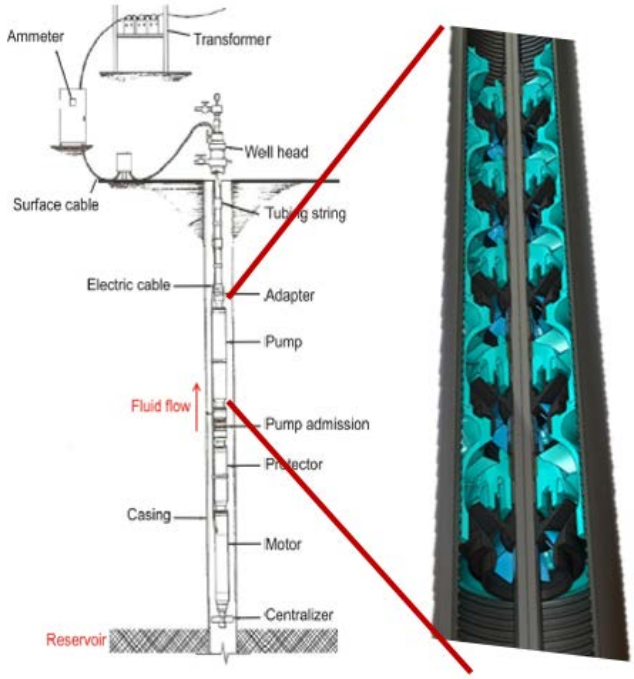

Figure 1.6: View of ESP sections, emphasizing the section this thesis covers. [1]

Pumps can range from radial to mixed flow. To handle higher GVF, an ESP may have mixed flow impellers. Figure 1.7 shows the change in impeller shape of a radial impeller to a mixed flow impeller. The flow path for a mixed-flow impeller is given an axial tilt to better handle a mixed flow of fluid-gas. This allows the impeller to operate in higher GVF without losing suction. A mixed flow impeller will also have balance holes to reduce the axial thrust from the impeller. Balance holes are located on the third and fourth impeller of Figure 1.7. The ESP modeled in this thesis has a mixed flow impeller.

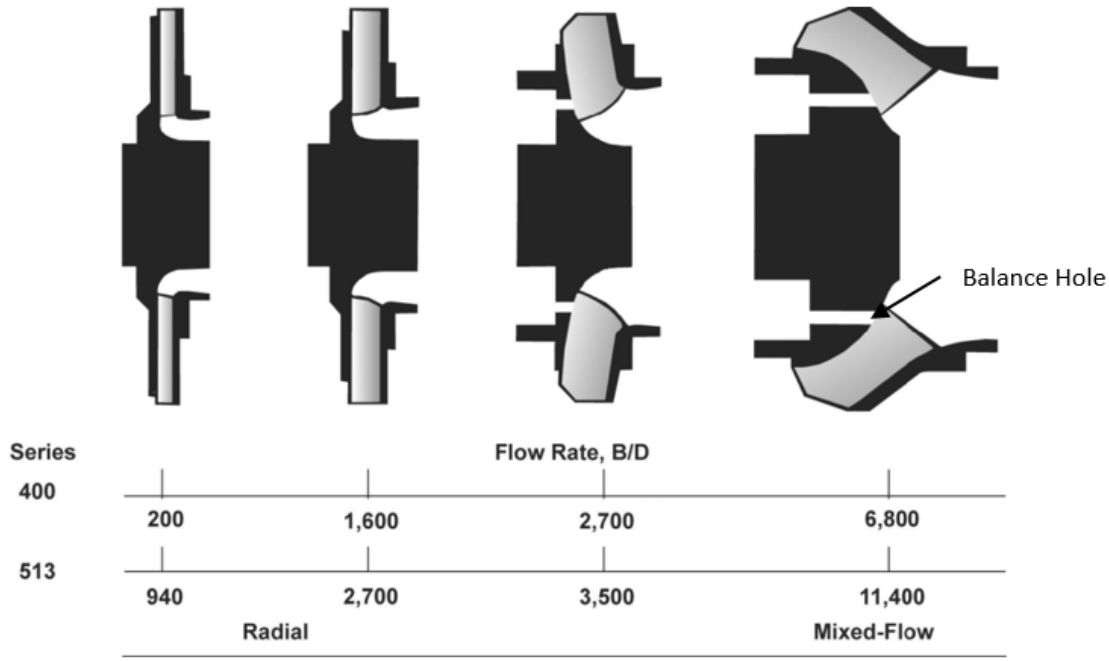

Figure 1.7: Radial vs. mixed flow impellers. [9]

Each pump stage has regions of different pressures. The lowest pressure is before the impeller intake, a middle pressure is located at the impeller exit, and the highest stage pressure at the diffuser outlet. These different pressures have to be restricted from flowing back through gaps between the rotating elements. Annular seals are used to restrict the flow. Annular seals are non-contacting which is important since the annular seals are restricting flow between a rotating rotor and fixed stator. This leaves a small circumferential fluid layer between the rotor and stator in the shape of an annulus. The thin fluid film transmits forces between the rotor and stator that are important for both the statics and rotordynamics of the rotor. A variety of properties affect the statics and rotordynamics. This includes the geometry, fluid properties, rotor speed, and inlet conditions.

As shown in Figure 1.8, Mixed-flow ESPs have three annular seals per stage: (1) An interstage seal restricts leakage from the back side of the diffuser to the impeller, (2) A front-wear-ring seal restricts leakage from the impeller exit to the front of the impeller, and (3) A rear-wear-ring seal that restricts flow from the impeller exit to the balance holes. Balance holes allow minor leakage back into the low pressure region of the impeller to decrease the axial load on the shaft. Together, these seals provide the necessary forces to support the rotor. The interstage seal is commonly considered to be the main supporting element. For this reason, the interstage seal is commonly referred to as a bearing in ESP literature. In this paper, it will be referred to as the interstage seal. Since the interstage has the smallest original clearance, it will be used to indicate rub. Enlarged clearances are assumed to have equal wear on all seals of the pump. In practice, the clearance increase due to wear will vary from seal to seal, this is neglected due to limited data. Also, wear will vary axially within a seal, but this possibility is also neglected.

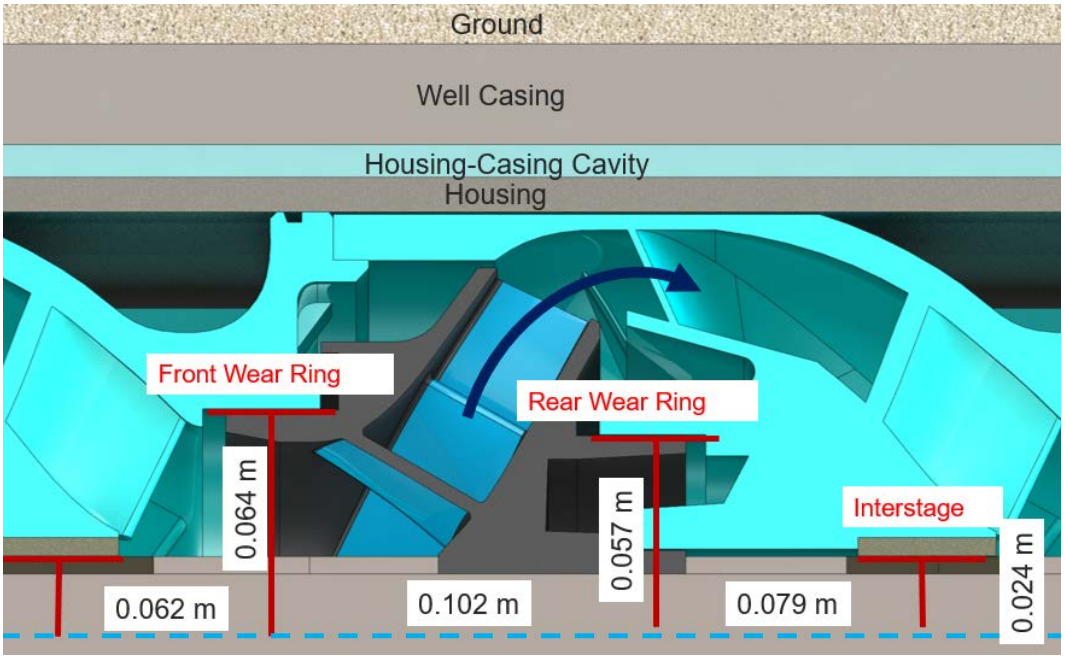

Figure 1.8: Example of mixed flow impeller. Seals are listed in red.

A seal with the lubricant flow in the laminar regime acts similar to a non-cavitated plain journal bearing. The seal has circumferentially-dominated flow and can be adequately modeled using the Reynolds equation. A seal in the laminar regime has a centering force that is strongly dependent on the seal's eccentricity [10]. In 1988, Nelson and Nguyen [11-12] predicted that liquid annular seals with turbulent flow also have eccentricity dependent stiffness and damping coefficients for eccentricity ratios greater than 0.5. The fluid in ESPs can have a large range of viscosities from 1 cP to 350 cP [13]. For simplicity, this thesis will focus on two viscosities, 1 cP and 30 cP. These two viscosities were given by a consultant that works with ESPs. The selection gives one viscosity in the laminar regime and one in the turbulent regime.

An eccentricity-dependent seal or bearing has the dynamic-coefficient matrix model

$$-\begin{Bmatrix} F_{\delta X}(\varepsilon_0) \\ F_{\delta Y}(\varepsilon_0) \end{Bmatrix} = \begin{bmatrix} K_{XX}(\varepsilon_0) & K_{XY}(\varepsilon_0) \\ -K_{YX}(\varepsilon_0) & K_{YY}(\varepsilon_0) \end{bmatrix} \begin{Bmatrix} \delta X \\ \delta Y \end{Bmatrix} + \begin{bmatrix} C_{XX}(\varepsilon_0) & C_{XY}(\varepsilon_0) \\ -C_{YX}(\varepsilon_0) & C_{YY}(\varepsilon_0) \end{bmatrix} \begin{Bmatrix} \delta \dot{X} \\ \delta \dot{Y} \end{Bmatrix} + \begin{bmatrix} M_{XX}(\varepsilon_0) & M_{XY}(\varepsilon_0) \\ -M_{YX}(\varepsilon_0) & M_{YY}(\varepsilon_0) \end{bmatrix} \begin{Bmatrix} \delta \ddot{X} \\ \delta \ddot{Y} \end{Bmatrix} \tag{1.2}$$

where K_{ij} is the dynamic stiffness, C_{ij} is the dynamic damping, M_{ij} is the dynamic virtual mass, $F_{\delta i}$ is the dynamic-force component, ϵ_0 is the eccentricity ratio ($\epsilon_0 = e_0/C_r$), δX is the rotor's relative dynamic displacement in the X direction, and δY is the rotor's relative dynamic displacement in the Y direction. These stiffness, damping, and mass terms depend on ϵ_0. The eccentricity-dependent reaction creates the need to know the correct static eccentricity ratio for accurate rotordynamic predictions.

A curved well will load the seals of the pump section and position the rotor to a new orientation. The position of the rotor with respect to the housing creates a new eccentricity that depends on the force-eccentricity loci of the seals, the number of seals, the stiffnesses of the rotor and housing, and the well's deviation. This new eccentricity can produce different stiffness, damping, and virtual mass terms for the seals. Also, if the static eccentricity is too large, the seals might rub.

ESPs in a horizontal well casing and surface applications need SEP analyses performed due to the effects from gravity. Gravity causes a lateral uniform force on the shaft. If the housing is not laser aligned, it may have a curvature. For this case, the ESP would need both the bend in the housing and gravity included in the model. The equilibrium position would then be calculated, and for surface applications will show how intermediate support points affects the rotordynamics. The influence of curvature and its

affect on the equilibrium position has not been previously accounted for in ESP rotordynamics.

1.2 Rotordynamics of ESP Pump Section Background

Al-Gheithi [14] presents the first ESP rotordynamics analysis that includes the pump section in 2004. Al-Gheithi's predictions are found using a Finite Element Model (FEM). The model of the ESP includes all three sections: the motor, seal-chamber, and the pump. The modeled ESP has 84 stages and has a length of 21.97 meters. The model includes the shaft, impeller weight, and seals. The model includes only the rotor, and not the housing. Rotor-only models ignore the housing vibrations and any joint rotor-housing modes of vibration. Al-Gheithi's model does not include all of the seals for the model. An 84 stage pump should include at least 168 seals. This is assuming a wear ring seal and an interstage seal for each stage. Al-Gheithi only includes 9 seal supporting elements in the pump section. Why the full number of supporting elements were not included is not stated. The coefficients used to model the seals are not speed or load dependent and are identical for every seal. The seals were modeled as plain journal bearings, the bearing dimensions are not stated. Overall, this study showed that modeling a full length ESP is possible, yet does not address key issues faced with ESP rotordynamics.

In 2009, Forsberg [15] presented data on a highly instrumented ESP with 50 accelerometers mounted on a 33 meter pump. Figure 1.9 shows the placement of the accelerometers on the ESP. The position was shown by integrating the acceleration data from the ESP. The pump housing vibrates at the 17th mode with an amplitude of 9 mm/s.

Forsberg's results show that an ESP's vibration cannot be accurately portrayed with a small number of sensors. The results also show that predicting the housing's vibration is important in ESP rotordynamics.

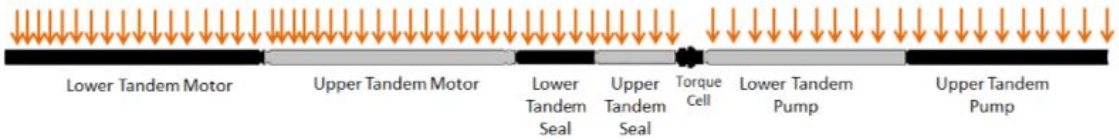

Figure 1.9: [13] ESP, tested by Forsberg, with accelerometers distributed along the housing to measure acceleration and response.

In 2014, Childs et al. [16] presented a primer on how to model the rotordynamics of the pump section of an ESP. The paper discusses the appropriate considerations for accurate modeling of ESPs. At the time, no code existed to reasonably predict eccentricities for all of the seals in the model. The model includes 80 seals all being eccentricity dependent. This included 20 stages with 4 seals in each stage including: (1) front wear ring, (2) rear wear ring, (3) impeller insert, (4) interstage. The seals are assumed to be loaded against one another to produce the eccentricities of 0, 0.4, and 0.8. The ESP model's dynamic characteristics showed a high eccentricity dependency. The curvature that ESPs could face was not included in the model. The analysis did not find the equilibrium position. Instead, for looking into the effects from eccentricity, chosen eccentricities were given for every seal uniformly in the model.

1.3 Static Equilibrium Position Background

Rotordynamic models containing eccentricity-dependent reaction forces require a static equilibrium position (SEP) to determine the rotordynamic coefficients. The SEP is the static position of the rotor. It is the position of the rotor that dynamic motion linear dynamic motion occurs around. Figure 1.10 shows an orbit of a rotor at one axial position around the SEP. For a given axial position, the SEP is the center of the rotor's dynamic path. Since the load is in the $-Y$ direction the position of the SEP with respect to the center of the supporting element is the eccentricity. e_X and e_Y represent the X and Y components of the eccentricity position. The eccentricity position can also be represented in polar coordinates as e_0 and ϕ, which are the corresponding eccentricity and attitude angle. ϕ is the angle between the eccentricity magnitude vector and the $-e_y$ vector. A $-Y$ load is seen with gravity loading. For vertical curvature the loading direction changes for every seal. Therefore, for vertical cases the relative rotor-housing position defines the rotor location. e_0 is calculated with

$$e_0 = \sqrt{\Delta X^2 + \Delta Y^2} = \sqrt{e_X{}^2 + e_Y{}^2} \tag{1.3}$$

Where ΔX and ΔY are the relative rotor-housing static displacements in the X and Y directions respectively. It is the same formula in terms of eccentricity components as relative rotor-housing displacement. Rotordynamic motion is elliptical with a major axis amplitude, a_{maj}, and a minor axis amplitude, a_{min}. The ellipse may have a lean of angle ψ that is the angle between the major axis and the X axis.

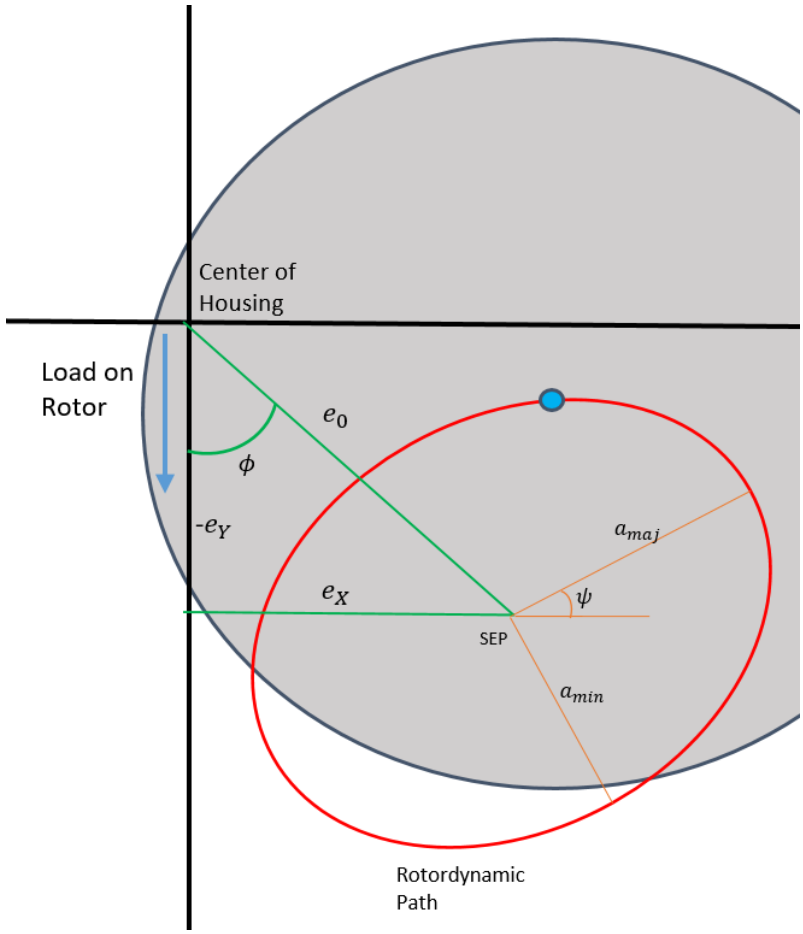

Figure 1.10: Rotor orbit around an SEP at one axial position.

The SEP is found by finding the configuration where the summation of forces in the entire rotor is equal to zero, similarly the lowest energy state. This is easy if the system is simply supported by two bearings, where half the rotor's weight is the force on the bearings. The eccentricity is then found from the force-eccentricity loci. If the system has more than two bearings, the solution is a set of non-linear equations, and must be solved using Newton-Raphson. A similar process is used to solve statically indeterminate beams.

In 1978, Holmes et al. [17] showed that radial misalignment for a rotor with more than two bearings, alters the rotordynamics of a multi-rotor system. Figure 1.11 shows the

model Holmes used. An offset in the second bearing affects the whole systems dynamics by changing the load on the remaining bearings. This affects the SEP of all the remaining bearings. The model is statically indeterminate with four bearings. Holmes finds the solution using a Runge-Kutta-Merson time transient method. To find the SEP, Holmes et al. then takes a time average of the rotor response. The time transient method process is computational demanding. Holmes et al. showed large changes in the dynamic response and stability by displacing the second bearing.

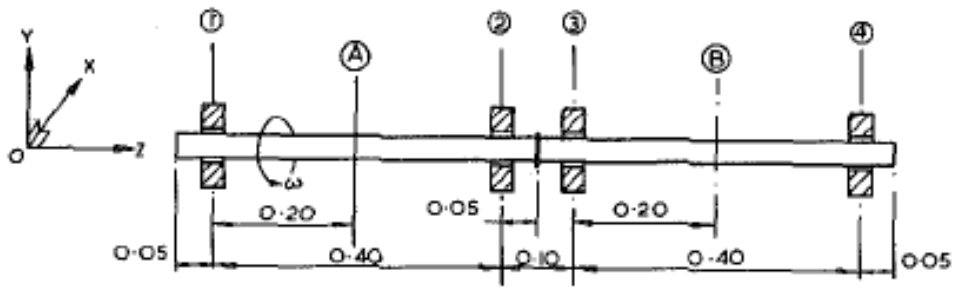

Figure 1.11: Holmes model to show the impact of bearing misalignment. Shaft A and shaft B are rigidly connected. [17]

In 1980, Hori and Uematsu [18] used a transfer matrix method approach to solve for the stability of a 2-rotor, 4-bearing system. The transfer matrix for the system is solved numerically using Newton-Raphson to find the stability. Hori and Uematsu found similar results to Holmes, namely, misalignment of bearings can lead to significant changes to stability.

In 1987, Gajan [19] developed a program that implemented a static indeterminate solver to find the rotor's equilibrium position. The rotordynamic coefficients at that rotor position were then implemented in a rotordynamic solver. His thesis furthered

rotordynamic codes in other areas as well. The new code included 4x4 stiffness and damping matrices which include the rotation and displacement at the seal. To the author's knowledge, these degrees of freedom had previously not been implemented into a rotordynamics code. Finally, the model included the effects from radial misalignment in a bearing. Gajan demonstrated his code's accuracy by comparing his predictions to past work done by Nikolajsen in 1980 [20]. Figure 1.12 shows the model used for verification of Gajan's analysis. Gajan's analysis does not account for a flexible housing. No code has yet addressed the issue of finding an equilibrium position for a system with eccentricity-dependent bearings and seals with a flexible rotor and flexible housing. Gajan remarks that "The next phase of this work is to include an option for pump housing flexibility to permit accurate modelling of vertical pumps which often have very flexible housings." This thesis is the continuation of Gajan's research to include the flexibility of the housing into modeling vertical pumps.

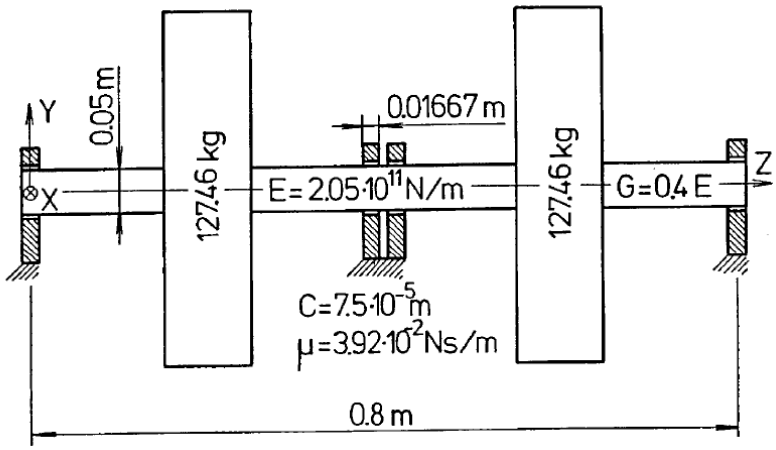

Figure 1.12: Model Gajan's Thesis used for verification of analysis. Center two bearings are the test bearings and were given lateral offsets. [19]

In 1988, Verhoeven [21] presented a paper outlying rotordynamic considerations for designing multistage centrifugal pumps. One section outlined the consideration of different loadings due to the seals reaction force. Without internal seals, the bearings load is half the rotor weight. In a multistage pump, part of the rotor's weight is carried by the internal seals. Verhoeven suggests using a quasi-static analysis with constant stiffnesses for the seals to simplify the analysis and eccentricity dependent stiffnesses for the bearings. Then the FEM is ran with simple spring connections to ground at the seal and bearing locations. The bearings' stiffnesses are iterated until convergence.

In 1998, Nikolajsen [22] revisited equilibrium position of rotors to compare three different ways of solving the problem. These three methods are: (1) the influence coefficient method, (2) the finite element method, and (3) the transfer matrix method. This thesis uses Nikolajsen's second method, a finite element model with a Newton-Raphson solver.

Currently, there doesn't exist an analysis that will be able to calculate the SEP of an ESP. Before this paper ESP rotordynamics has assumed a straight shaft. Childs et al. in 2014 [16] showed that uniformly offsetting all of the seals creates changes to stability and synchronous response in an ESP pump section.

2. STATEMENT OF WORK

This thesis is to create an analysis suitable for determining an SEP of an ESP pump section. The analysis is to fill the gap on housing curvature SEP that is needed for ESPs unique conditions of curved wells. The analysis developed for this thesis continues Gajan's work on determining SEPs. It is expanded by: (1) including eccentricity-dependent seals, (2) introducing the housing and its flexibility into the model, (3) iteratively solving for only the stations that are eccentricity dependent, based off the work by Hu et al. in 2004 [23], (4) specifying the housing's shape with added virtual forces.

The analysis accepts rotational-axis-symmetric model for the seals: the rotor reaction force must be in the same direction and magnitude for all angles of the rotor position. Seals in an ESP are generally rotational-axis-symmetric due to erosion. The model has inputs of fixed offsets or housing displacements. Probabilities of an offset due to random housing assembly error cannot be included. The code also assumes the shape of some contacting points on the housing are known. The code will solve for any housing station positions if a position is not prescribed. This code solves for the unknown static rotor configuration in an ESP.

A sample ESP is presented in Section 5 as an example for the program. The sample has the equilibrium position calculated for 4 different configurations: (1) horizontal fixed straight housing, (2) intermediate supported housing, (3) vertical housing with curvature, (4) 3D helically bent housing. All cases have the seals changed viscosity and clearance. This is to investigate the impact from fluid change and wear.

3. METHOD

3.1 Statics Derivation

The equilibrium configuration occurs when the constant forces and moments sum to zero for the system. This requirement yields the equation

\[0=\sum\limits_{a=0}^{n}{{{F}_{a}}}\] (3.1)

where $\{F\}$ is the force vector containing all forces and moments at node a in the system FEM. This includes both the internal-shear forces/moments and external-bearing-reaction forces/moments. This equation are the backbone for a statics problem. $\{U\}$ is defined as the vector containing the positions and angles of the rotor and housing. The rotor/housing and some seals are considered to have constant stiffness. These structural elements are removed from $\{F\}$ and replaced with a stiffness and displacement which gives

$$[K_L]\{U_{Eq}\} = \{F_E\} \tag{3.2}$$

where $[K_L]$ is the stiffness matrix of the structural elements. $\{U_{Eq}\}$ is the equilibrium position vector of the rotor around which the dynamic motion of the rotor occurs. $\{F_E\}$ is the external time independent force vector. In the case for finding the equilibrium position vector, $\{U_{Eq}\}$ is the unknown. $\{U_{Eq}\}$ is solved for by a left hand inverse of the matrix $[K_L]$ yielding

$$\{U_{Eq}\} = [K_L]^{-1}\{F_E\} \tag{3.3}$$

Some supporting elements in an ESP pump may exhibit non-constant stiffness with respect to eccentricity, this problem then is non-linear. A numerical approach is needed to

find $\{U_{eq}\}$. The one chosen for this paper's analysis is the Newton-Raphson technique. Hu et al.'s method is used to split the stations to separate equations. One for the non-linear stations, $\{U_{NL}\}$ and one for remaining stations, $\{U_L\}$. This creates less stations that need to be iteratively solved for.

The numerical approach used to find $\{U_{NL}\}$ is the Newton-Raphson technique. This numerical analysis iterates through a function while trying to set a vector to zero. The vector in this case is $\{G\}$ which contains the error in the non-linear station force balance equation. The vector $\{G\}$ is

$$\{G\} = [C_1]\{U_{NL}\} - [C_2]\{F_L\} + \{F_{NL}(\{U_{NL}\})\} \tag{3.4}$$

where $[C_1]$ and $[C_2]$ are constant matrices through the iterations, $\{F_L\}$ is a vector of forces on all non-eccentricity-dependent stations, and $\{F_{NL}()\}$ is a vector of forces from the eccentricity-dependent seals that depend on the displacement. The definition of these can be found in Appendix A. $[C_1]\{U_{NL}\}$ is a vector of forces from the non-linear stations displacement, $[C_2]\{F_L\}$ is a vector of forces on the non-linear stations from the linear stations, and $\{F_{NL}(\{U_{NL}\})\}$ is the vector of forces from the supporting element. The Jacobian of G is

$$[J] = [C_1] + [K_B(U_{NL})] \tag{3.5}$$

where $[K_B(\{U_{NL}\})]$ is the matrix containing the bearing stiffnesses of the supporting elements at displacement $\{U_{NL}\}$. Eq. (3.4) and (3.5) are then used to find $\{U_{Eq}\}$. The first guess is found by setting the non-linear seals to a temporary large linear stiffness of $1 *$

10^{12} N/m. This sets the rotor to center at every non-linear bearing. , then using eq. (3.3). $\{U_{Eq}\}$ is then iteratively solved for using

$$\{U_{n+1}\} = \{U_n\} - [J^{-1}]\{G\} \tag{3.6}$$

Where $\{U_{n+1}\}$ is the guess for the following iteration and $\{U_n\}$ is the current guess. Convergence is found when G is within a small margin of 0.

3.2 Setting Curvature of the Housing Derivation

A deviation in the housing straightness is modeled as an added force to the system. This added force is equal to the force applied to the rotor from displacing the supporting elements the desired amount. The added force is equal to

$$\{F_A\} = f(\{U_D\}) \tag{3.7}$$

where $\{U_D\}$ is the desired displacement. Assuming the supports to be linear then $\{F_A\}$ can be rewritten as

$$\{F_A\} = [K_S]\{U_D\} \tag{3.8}$$

where $[K_S]$ is the matrix containing only the seal stiffnesses. The rotor's added force can then be added to the general linear static equilibrium equation to obtain

$$\{U_{eq}\} = ([K_S] + [K_R])^{-1}\{F_A\} \tag{3.9}$$

where $[K_R]$ is the stiffness matrix for the rotor.

The theorem for the inverse of the sum of two matrices is applied to prove that the desired displacement is still included [24]. The theorem is that if $[K_S]$ is invertible, $[K_R]$

is not invertible, and $([K_S]+[K_R])$ is invertible then it is possible to expand $([K_S]+[K_R])^{-1}$ to

$$\begin{aligned}([K_S]+[K_R])^{-1} &= [K_S]^{-1} - [K_S]^{-1}[K_R][K_S]^{-1} \\ &+[K_S]^{-1}[K_R][K_S]^{-1}[K_R][K_S]^{-1}....\end{aligned} \tag{3.10}$$

Plugging in the expanded form into eq. (3.8) yields the first term as $[K_S]^{-1}\{F_A\}$ which is equal to $\{U_D\}$. The remaining parts will contribute much less to the overall displacement. It also depends on the "shape" of the forces on the rotor.

This method is applied to this analysis by adding a near rigid connection to the housing at the known FEM station. Eq. (3.8) is used to determine an applied force at the same station to set the displacement. For this method to work, an assumption is made that the stiffness of the added housing support must be much greater than the support between the housing and rotor. This is done by making the support 10^12 N/m. The advantage of this method is the support between the rotor and housing can be non-linear without recalculating the added force to the model.

3.3 Code Outline

First, the input data for the model is collected. This includes the: desired speed, rotor/housing model, desired SEP positions, linear seals, bearings, static forces, and added masses. The program cycles through all of the eccentricity-dependent seals. Each seal is run for 10 different eccentricities, ranging from 0-0.9 in increments of 0.1 at the requested speed.

The radial forces that do not depend on speed or eccentricity are added to a force vector $\{F_s\}$. This includes the gravity forces, static forces, and loading from the housing curvature. Explanation for how gravity force was calculated is found in Appendix B. The eccentricity-dependent seals are given a spline profile relating the eccentricity to the centering force and stiffness. This spline profile is used for interpolation during every iteration in the Newton-Raphson solver.

An initial linear guess is made by setting every non-linear bearing stiffness to 10^{12} N/m. This gives a linear system and Eq. (3.3) is used to find an initial displacement for all stations. For the case where all bearings and seals do not depend on their eccentricities, the code skips the Newton-Raphson algorithm and uses the initial linear guess answer as the solution. If there are any eccentricity-dependent bearings or seals, the code continues by finding $[C_1]$ and $[C_2]$ of Eq. (3.4). The code then starts the Newton-Raphson loop.

The main loop to determine the equilibrium position begins. The last loop or initial conditions are used to determine the stiffnesses and forces of the eccentricity-dependent bearings and seals for the current loop. Next the code develops the function G and J of Eq. (3.4) and (3.5). Eq. (A.21) is then used to solve for the next guess. If the Root Mean Squared (RMS) of G is below 0.001, the code stops and the next guess is the final solution.

Once the final solution is found for the coordinates at rotor locations with nonlinear reaction forces, Eq. (A.13) is used to solve for the remaining coordinates. The stiffnesses for all of the bearings at the found equilibrium position are saved to a text file for later use in rotordynamics. The static equilibrium position is saved to a text file to be displayed as an output. Figure3.1 shows a simplified flow diagram for the code.

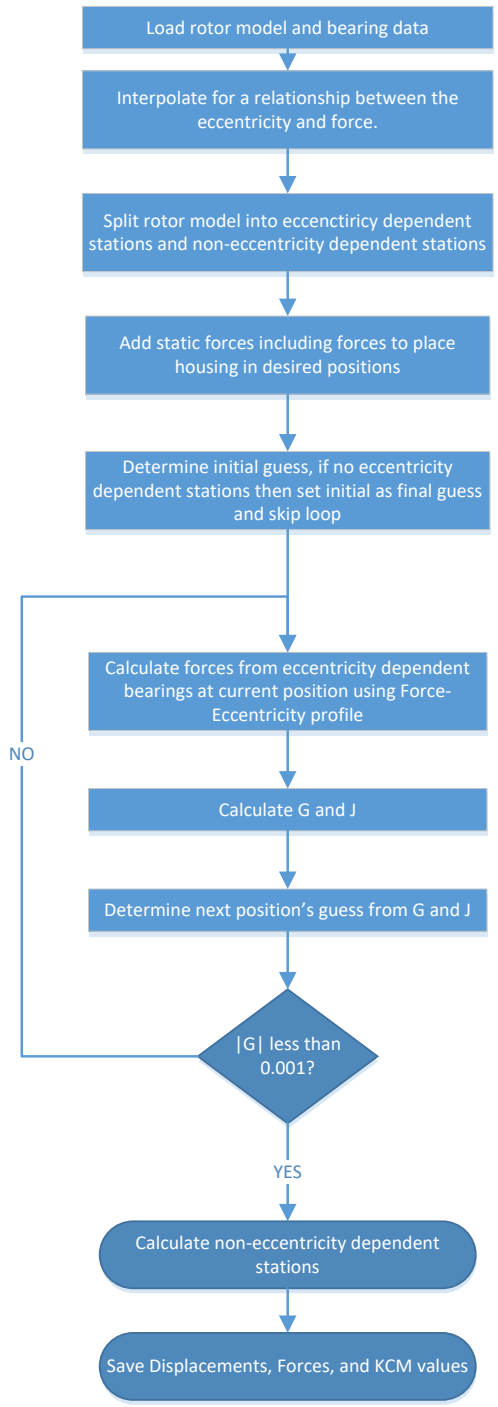

Figure3.1: Flow chart for static equilibrium position analysis.

4. CODE VALIDATION

This thesis's output agreed with Gajan for cases that were available. No comparable predictions are available for a flexible housing and non-linear seals. For code validation two models are considered: (1) a one line model with a rotor held by 5 eccentricity dependent seals and (2) a two line model with 20 constant stiffness seals. Static positions of the rotor are predicted. The position is displayed for the requested speed.

4.1 Gravity Loading on Multiple Eccentricity-Dependent Seals

The first model to show the validity of the equilibrium position analysis is a rotor supported by 5 seals with eccentricity-dependent stiffness coefficients. The model is presented in Figure 4.1. The elastic modulus is $2.048\ GPa$ and the density of the rotor is $77{,}090\,\frac{kg}{m^3}$. The length of the rotor is 1.02 m (40 in) with a diameter of 50.8 mm (2 in). The 5 seals are plain annular seal with the parameters listed in Table 4.1. Pre-swirl ratio is defined as

$$PSR = \frac{u_0}{\omega} \tag{4.1}$$

Where u_0 is the inlet flow circumferential velocity, and ω is the rotational speed of the rotor. The force and stiffness coefficients are presented for 10 different eccentricities in Table 4.2. This example only has a minor change in stiffness coefficients from centered to 0.9 ϵ_0.

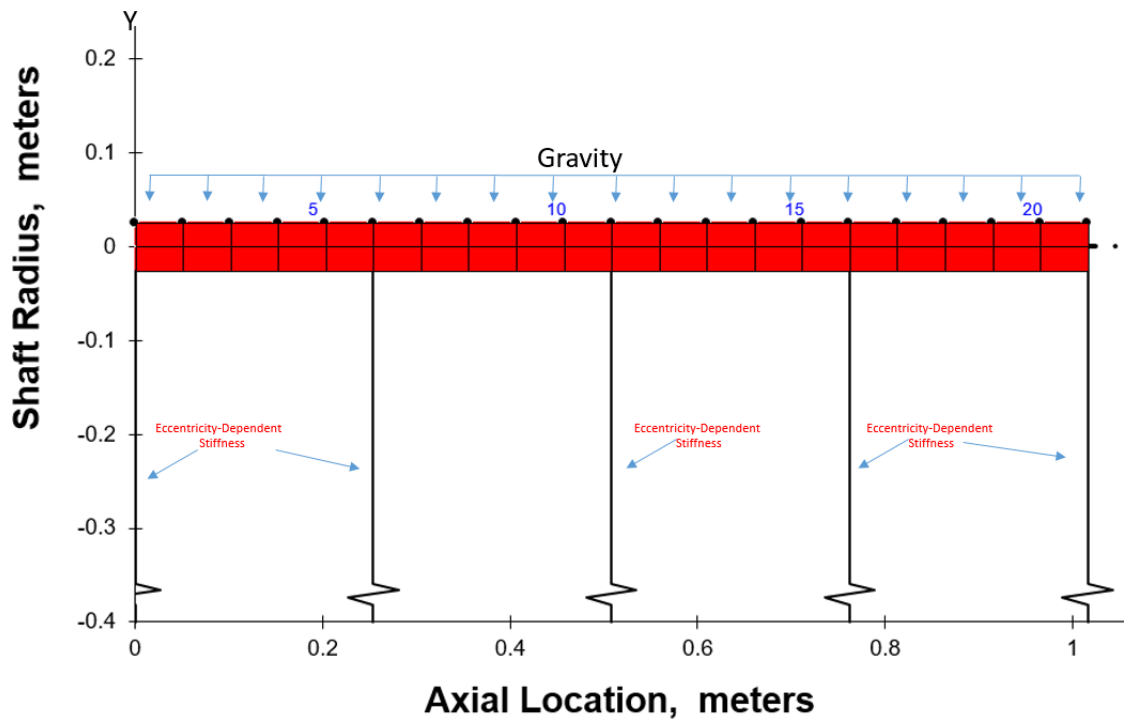

Figure 4.1: Model for proving distributed loading. Gravity is acting in the negative *Y* direction.

Table 4.1: Seal Properties for single line validation model. Running speed of 3600rpm

Parameters	**Values**
Diameter	0.10 m
Length	0.0254 m
Clearance	0.19 mm
Viscosity	0.54 cP
Differential Pressure	2.4 bar
Preswirl Ratio (PSR)	0.5
Density	988 kg/m3

Table 4.2: Stiffness with respect to eccentricity for validation model. Running speed of 3600rpm.

ϵ_0	K_{XX}	K_{XY}	K_{YX}	K_{YY}	F_X	F_Y
-	N/m	N/m	N/m	N/m	N	N
0.0	7.15E+05	4.84E+05	-4.84E+05	7.15E+05	2.64E-02	6.33E-02
0.1	7.15E+05	4.88E+05	-4.85E+05	7.15E+05	8.33E+00	1.31E+01
0.2	7.14E+05	5.01E+05	-4.88E+05	7.13E+05	1.80E+01	2.71E+01
0.3	7.13E+05	5.24E+05	-4.94E+05	7.09E+05	2.78E+01	4.07E+01
0.4	7.06E+05	5.77E+05	-5.11E+05	6.07E+05	3.82E+01	5.37E+01
0.5	6.75E+05	6.64E+05	-5.58E+05	5.14E+05	5.01E+01	6.36E+01
0.6	6.63E+05	7.47E+05	-6.29E+05	6.38E+05	6.33E+01	7.25E+01
0.7	6.73E+05	9.41E+05	-6.67E+05	8.39E+05	7.79E+01	8.46E+01
0.8	6.88E+05	1.48E+06	-6.12E+05	6.45E+05	9.68E+01	9.84E+01
0.9	6.69E+05	4.44E+06	-8.76E+05	3.12E+05	1.40E+02	1.08E+02

The input force for this model is gravity acting laterally in the $-Y$ direction. The rotor weighs 159 N (16.2 kg). The five seals then oppose gravity with a reaction force, creating an equilibrium position. The total external forces acting on the rotor, gravity and seal reaction forces, are presented in Figure 4.2. The large positive forces are the seal reaction forces balancing the large negative forces which are gravity forces. The blue forces are in the X direction are due to the cross coupled stiffness in the bearings. Excluding error, these forces in the X and Y directions sum to zero to satisfy the statics equations. At convergence, the summation of external forces in the X and Y directions is -$2\text{x}10^{-4}$N and $-4.9\text{x}10^{-4}$N receptively. These residual forces are small in comparison with the weight of 159N. The residual forces come from rounding error and interpolation error.

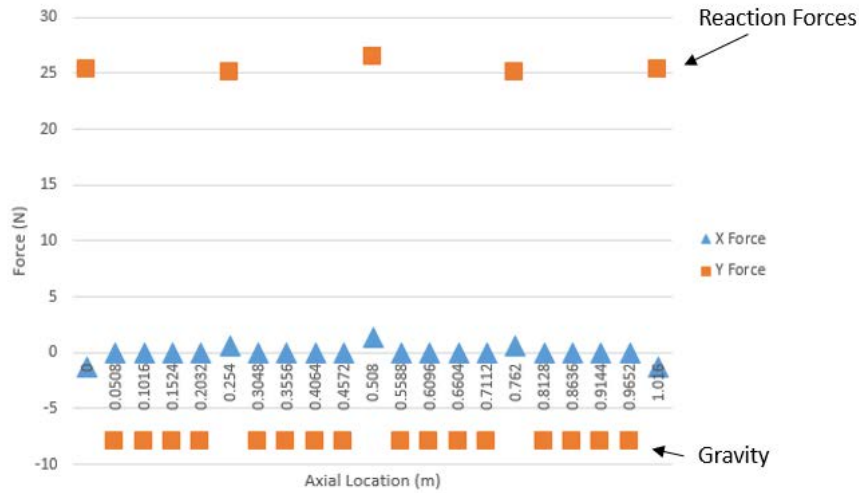

Figure 4.2: Forces including gravity and seal reaction vs. Axial Position

The displacement in the *X* and *Y* directions is seen in Figure 4.3. The displacement of the rotor is a slight downward curve in the load direction (-*Y*). The *X* direction is relatively straight and positive. This indicates a positive attitude angle.

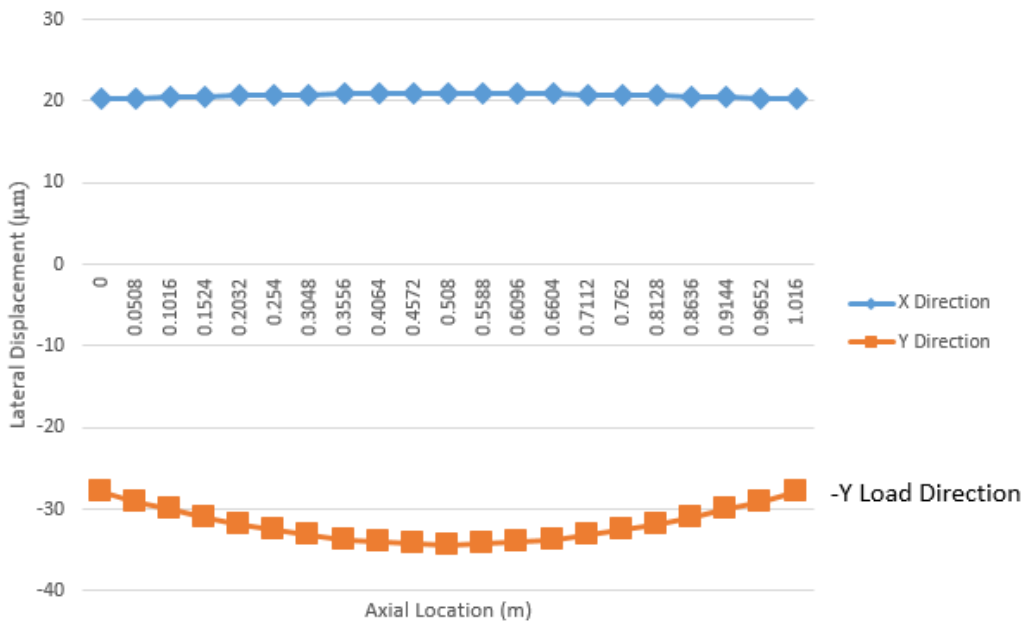

Figure 4.3: Displacement of the Rotor for Validation model 1. Load is in the –*Y* direction.

Since this analysis is non-linear, an exact solution is never obtained. Instead, the solver terminates at a determined margin of error. Convergence occurs when the solution adequately approaches the correct solution. The following two ways can be used to determine convergence (1) If the error vector, {G}, is sufficiently close to zero or (2) The deviation in the inputs, $\{\epsilon_0\}$ and $\{\phi\}$, after each iteration has diminished. {G} is the vector that the Newton-Raphson solver is trying to reduce to zero, listed in section 1.5. The error per iteration is shown in Figure 4.4. The subscript RMS means the root mean squared of the vector. The subscript MAX means it is the largest value in the vector. The increase in error for the RMS and MAX eccentricity ratio up to iteration 5 is due to the attitude angle, ϕ, needing to converge. At iteration 5 the solver starts to rapidly converge onto a solution with a quadratic rate of convergence for both the inputs and error vector. G_{RMS} is used for

the convergence criteria in this program due to the inclusion of both ϵ_{0RMS} and ϕ_{RMS}. A value of $1 * 10^{-6}$ is the cutoff for convergence for G_{RMS}.

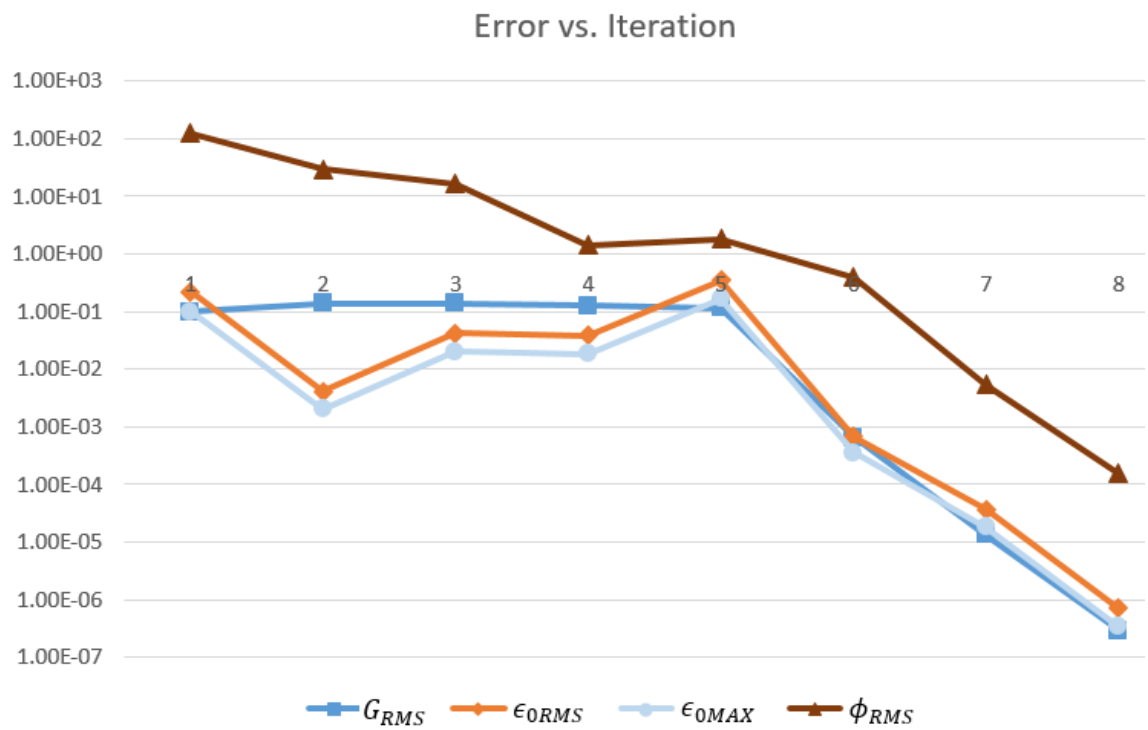

Figure 4.4: Convergence graph for validation model 1. G is the force vector at the seals.

4.2 Uniform Curvature Multi-Seal Model

Figure 4.5 shows the next simple model. The model consists of a 2.4 m long rotor with an equal length housing. The rotor diameter is the same as previous examples at 50.8 mm. Twenty seals with constant stiffness are distributed equally along the length of the rotor and are connected to the housing. These seals provide the centering force to the rotor and their reaction forces determine the position of the rotor. Two cases are run using the

two different stiffness coefficients seen in Table 4.3. The housing is given a set position so its flexibility and connection to ground is not of concern.

Table 4.3: Seal stiffness coefficients for multi-seal supported rotor.

Seal	Kxx (N/m)	Kxy (N/m)	Kyx (N/m)	Kyy (N/m)
With Cross	1.75×10^7	17500	-17500	1.75×10^7
No Cross	1.75×10^7	0	0	1.75×10^7

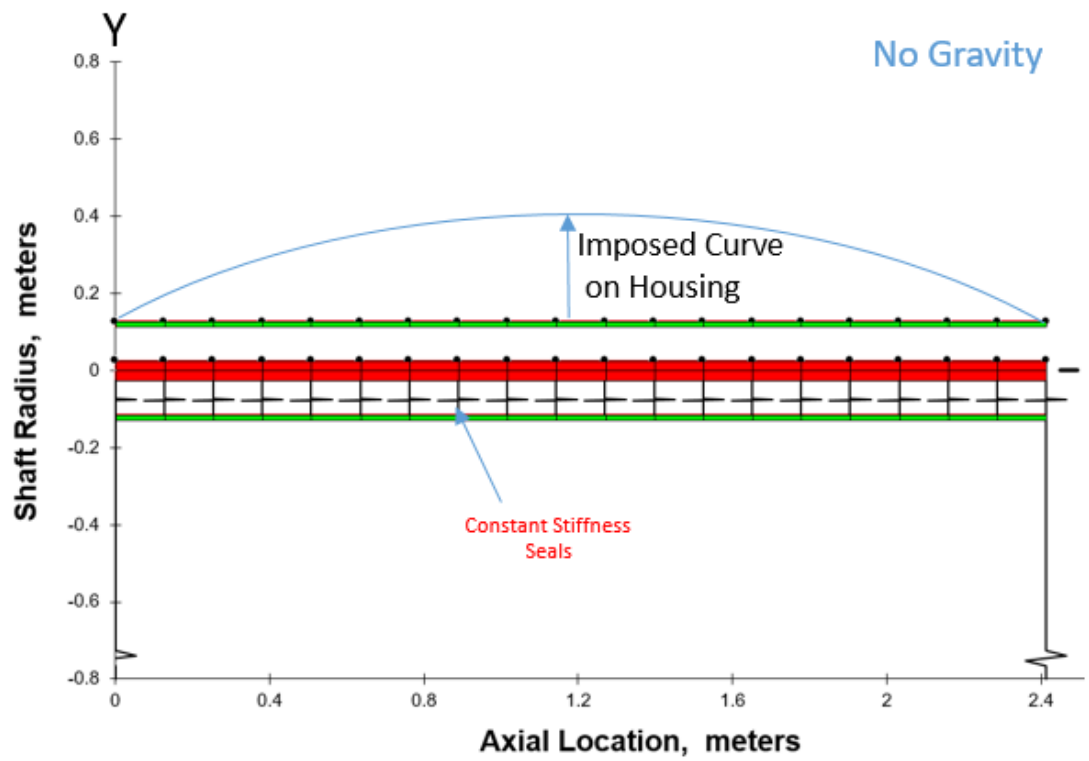

Figure 4.5: Basic two line model to show the impact of curvature.

This model's housing is then subjected to a curvature of 1 DOC. Figure 4.6 shows the forces from the housing curvature, which is the displacement of the housing times the

stiffness coefficients. The rotor receives forces equal to the amount of displacement in the seal due to the housing movement. If the housing is moved to its desired position, since the rotor is connected to the housing, the rotor will follow. The static shape can be seen below in Figure 4.7. The housing is at the imposed shape, while the rotor closely follows the housing shape.

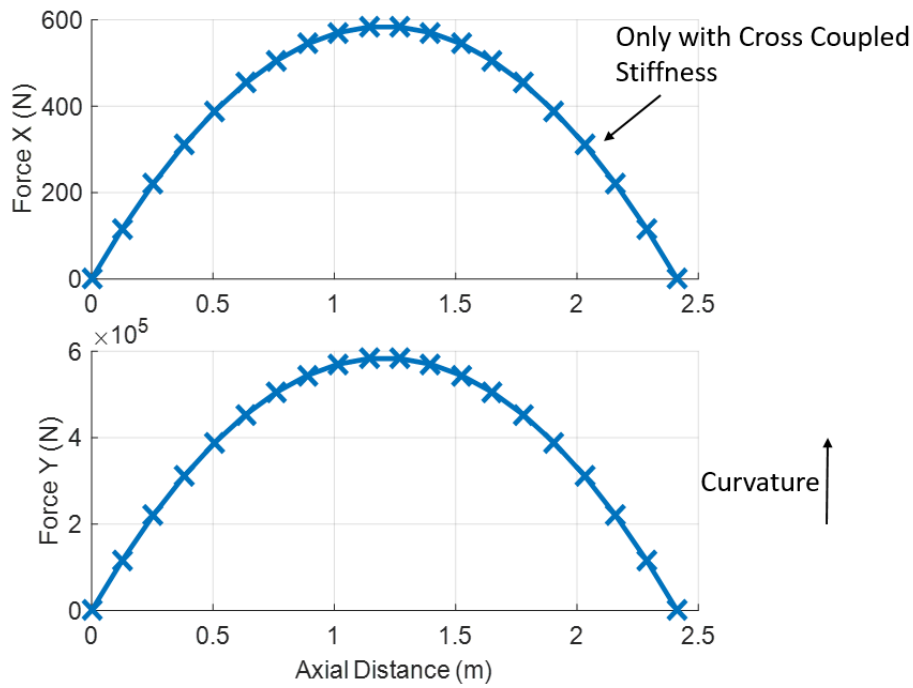

Figure 4.6: Applied force onto rotor from a constant curvature. This force profile is with cross coupled stiffness. Force in the *X* direction is zero for all axial positions without cross coupled stiffness.

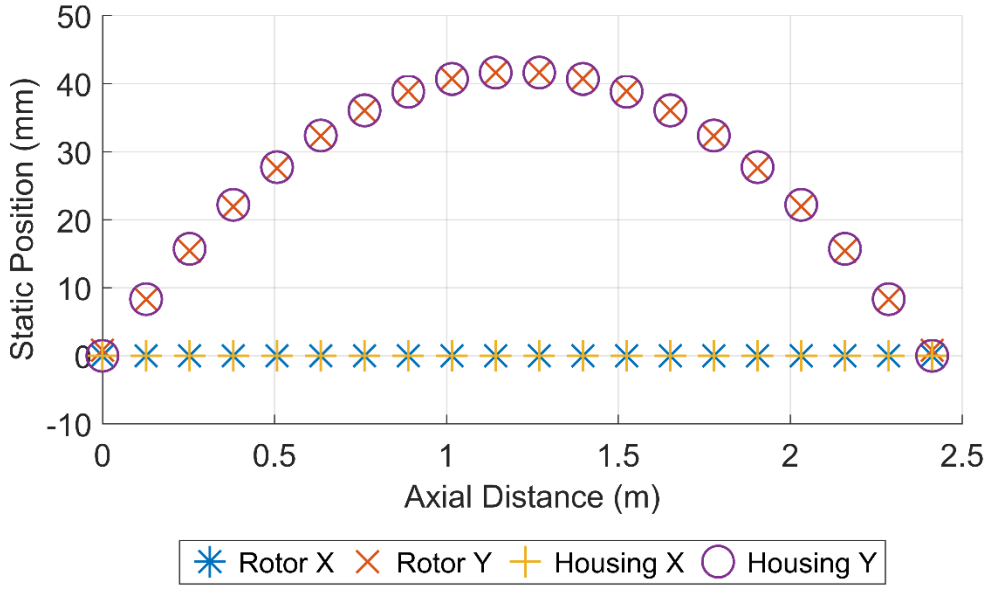

Figure 4.7: Static equilibrium position of basic curvature. Solution is the same with and without cross coupled stiffness.

Since the scale of the housing length is much greater than the bearing clearance there is no noticeable difference between the rotor and housing while showing the overall shape. By taking the difference of the housing center line and rotor position the offsets on each bearing can more clearly be seen. Figure 4.8 shows the relative rotor-housing shape in the X and Y directions, listed as ΔX and ΔY respectively. The static position has a wave profile in the Y direction independent of cross coupling. Also included in the figure is the same model with forty seals instead of twenty. This creates no changes to the relative profile. The "wave" shape happens in all cases of a housing curvature even with linear seals. This leads to the conclusion that the relative profile seen is from having housing curvature imposed through springs onto a rotor.

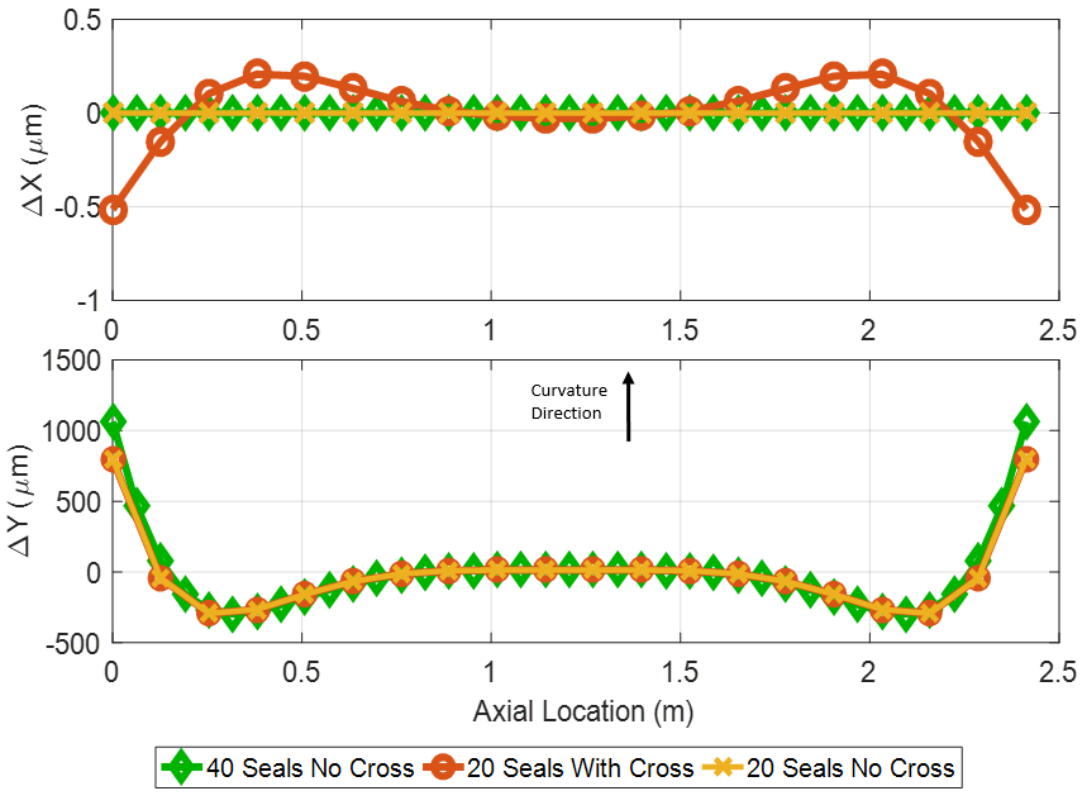

Figure 4.8: Calculated relative rotor-housing eccentricities due to an imposed housing curvature on a rotor with linear seals.

5. PREDICITIONS FOR SAMPLE ESP

5.1 ESP Pump Section Model

The model is the same sub-sea pump model used in the paper by Childs et al. [16]. Figure 5.1 shows 5 stages of the 20 stage model. The 20 stage ESP has a 0.2 m (8.25 in) diameter impeller and is mainly used for sub-sea oil production. Figure 5.2 shows the full model in XLTRC^2 which is the analysis interface. The pump length is 5.26 m with each stage being 0.24 m in length. There is a 0.20 m segment at each side of the twenty stages transitioning to a pinned connection to the housing. The housing is twice the length of the rotor to reproduce the flexibility of an ESP with other ESP components. The housing is pinned to ground. The diameter of the shaft is 38.1 mm. The model takes into account the flexible housing of an ESP. The inner diameter of the housing is 0.241 m and has a thickness of 9.53 mm. The total mass of the rotor is 196 kg.

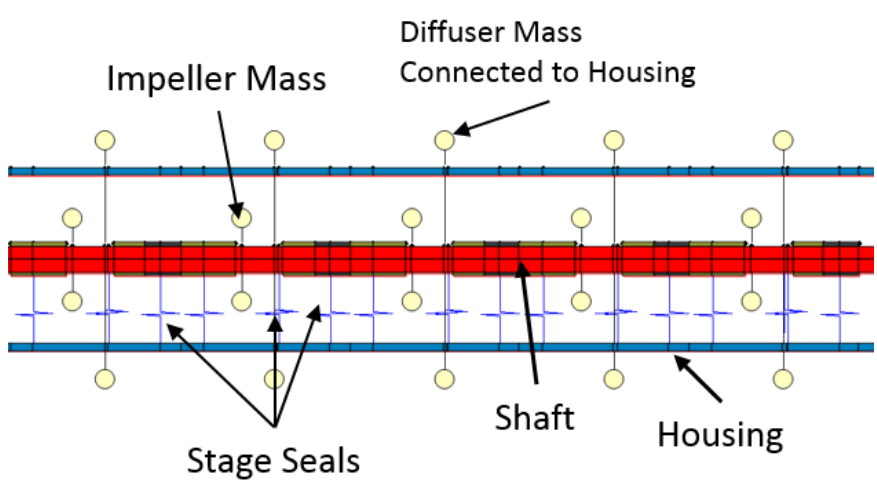

Figure 5.1: Side view for 5 stages of Sample ESP model

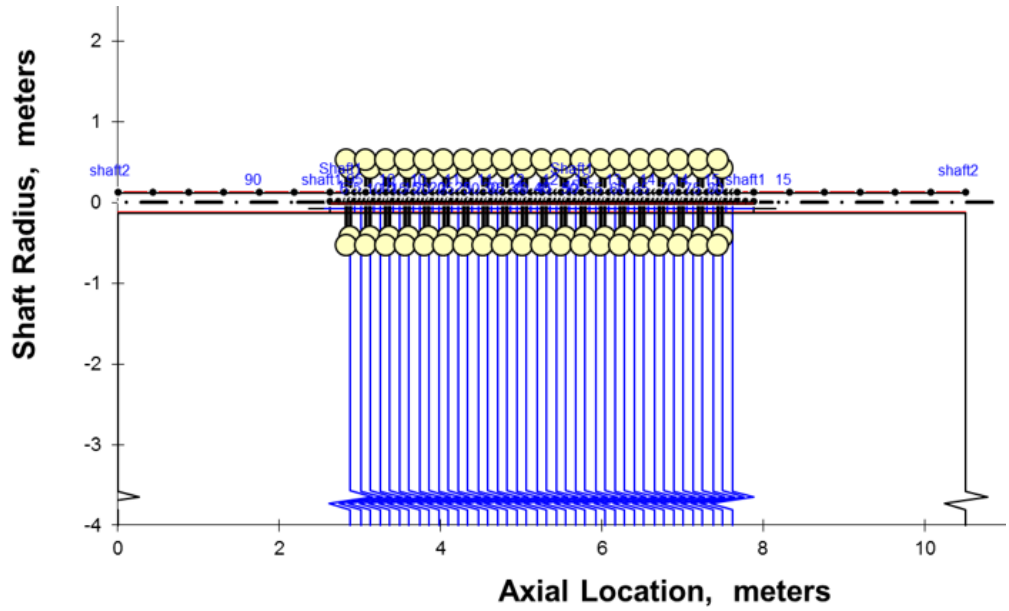

Figure 5.2: Full model of ESP in XLTRC. All blue lines are seal locations.

In the model, both the rotor and housing are pinned at their ends. The rotor is pinned to the housing, which requires that the rotor be at the same lateral position as the housing's centerline. The rotor model's synchronous excitation forces arise from: bent shaft excitation, hydraulic imbalance, mechanical imbalance of the impeller, and mechanical imbalance of the rotor. Gravity does not impact the equilibrium for the vertical cases. The horizontal model includes buoyancy of the rotor. This buoyancy is the internal volume of the rotor and impellers times the density of the process fluid. The impeller fluid mass is an added dynamic mass to the model. The impeller fluid mass is equal to the volume of the fluid impeller cavity of the impeller times the density of the process fluid.

The three seals shown in Figure 1.8 are included on each stage, namely the: front wear ring, rear wear ring, and interstage seal. All three seals are modeled with XLAnSeal, which was developed by Zirkelback, N., and San Andrés, L in 1996 [25]. Table 5.1 lists

the dimensions of the three seals. XLAnSeal predictions have been compared to test data at a viscosity of 30 cP [26] with similar clearance ratios and length ratios. The output for force vs. eccentricity can be found in Appendix D. The moments generated from the bearings and seals are removed from the eccentricity-dependent bearings and seals due to their small influence on the centering force. For the force vs. eccentricity predictions see Appendix C. There are four different seal configurations analyzed for this ESP pump.

Table 5.1: Seal geometry for a single ESP stage

Seal	**Length (mm)**	**Diameter (mm)**	**Original C_r (μm)**	$\frac{L}{D}$	**ΔP (bar)**
Front Wear Ring	25.0	128	231	0.20	1.69
Rear Wear Ring	26.0	114	348	0.23	1.69
Interstage	38.3	47.8	127	0.80	2.31

Table 5.2 lists the four configurations and their respective abbreviations. Two different parameters are changed in this analysis. The radial clearances are enlarged to 3X the original size to simulate wear. The viscosity of fluid is varied between 1 cP and 30 cP to investigate the effects from turbulent and laminar flow. All cases for the thesis are ran for the operating speed of 3600 rpm. 3X 1 cP has swirl-brakes included in the model to stabilize the response. Swirl-brakes reduce the circumferential flow entering the seal. This lowers the cross-coupled stiffness which improves stability. Table 5.3 lists the pre swirl for each seal in the model when swirl brakes are implemented.

Table 5.2: Different seal configurations for sample ESP pump

Abbreviation	Defined Case
1X 1cP	Original Clearance for all seals. 0.92 cP fluid to simulate turbulent flow. Fluid density: 998 kg/m^3
1X 30cP	Original Clearance for all seals. 30 cP fluid to simulate laminar flow. Fluid density: 860 kg/m^3
3X 1cP	Enlarged Clearance to 3X the original simulating wear for seals. 0.92 cP fluid to simulate turbulent flow. Fluid density: 998 kg/m^3. Includes swirl-brakes
3X 30cP	Enlarged Clearance to 3X the original simulating wear for seals. 30 cP fluid to simulate laminar flow. Fluid density: 860 kg/m^3

Table 5.3: PSR, eq. (4.1), for seals in model.

Seal	No swirl-brakes	With wear-ring Swirl-brakes
Front wear ring	0.7	0.1
Rear wear ring	0.7	0.1
Interstage	0.4	0.4

These predictions are to show trends on how different loadings affect the statics and rotordynamics. Unfortunately, no test data exists on ESPs in curved sections or the shaft rotordynamics under gravity loading. Hence, there are no comparisons between predictions and test data. ESPs can sit at many different orientations ranging from vertical to horizontal. The two extremes of horizontal and vertical are considered in the following predictions. For any angle in between the gravity should be scaled based on the angle.

5.2 Statics of a Horizontal ESP

For this section, the housing is set to a completely horizontal straight orientation, there is no curvature of the housing. Therefore, the rotor is only unknown in the SEP, the housing does not play a role since all lateral locations are set to zero. The influence of having intermediate supports is shown in the following section 3.3. Section 3.3 includes the rotor weight and buoyancy. The rotor weight is 1923 N. The buoyancy for 1 cP is 252 N and 217 N for 30 cP. This yields a total downward force of 1671 N for 1 cP and 1706 N for 30 cP.

Figure 5.3 shows the static position of a horizontal ESP with a process fluid of 1 cP. The 1X 1cP results in a peak relative displacement of $67.12\ \mu$m. The original clearance is $127\ \mu$m. The maximum eccentricity ratio in a seal is then 0.53 of the clearance. Rub due to static displacement should not be an issue in this ESP configuration. The rotor stays at approximately the same eccentricity for all seals, only the ends return to zero eccentricity. This is seen for all horizontal cases. For 1X 1cP, the *X* displacement is higher than the *Y* displacement. The rotor offset in the *Y* direction, which is the direction of the load is about 80% the *X* direction displacement indicating a near $51°$ attitude angle. For 3X 1cP the maximum relative displacement is $290.5\ \mu$m. The minimum clearance is $381\ \mu m$ making the maximum eccentricity ratio of 0.76. This has considerable clearance to the wall. 3X 1cP has more -*Y* direction relative displacement than *X* direction, indicating a decrease in cross-coupled stiffness from 1X 1cP. This decrease in cross-coupled stiffness is due to the swirl-brakes lowering the cross-coupled stiffness. ESPs for this configuration may operate at a considerable eccentricity ratio if mounted horizontally.

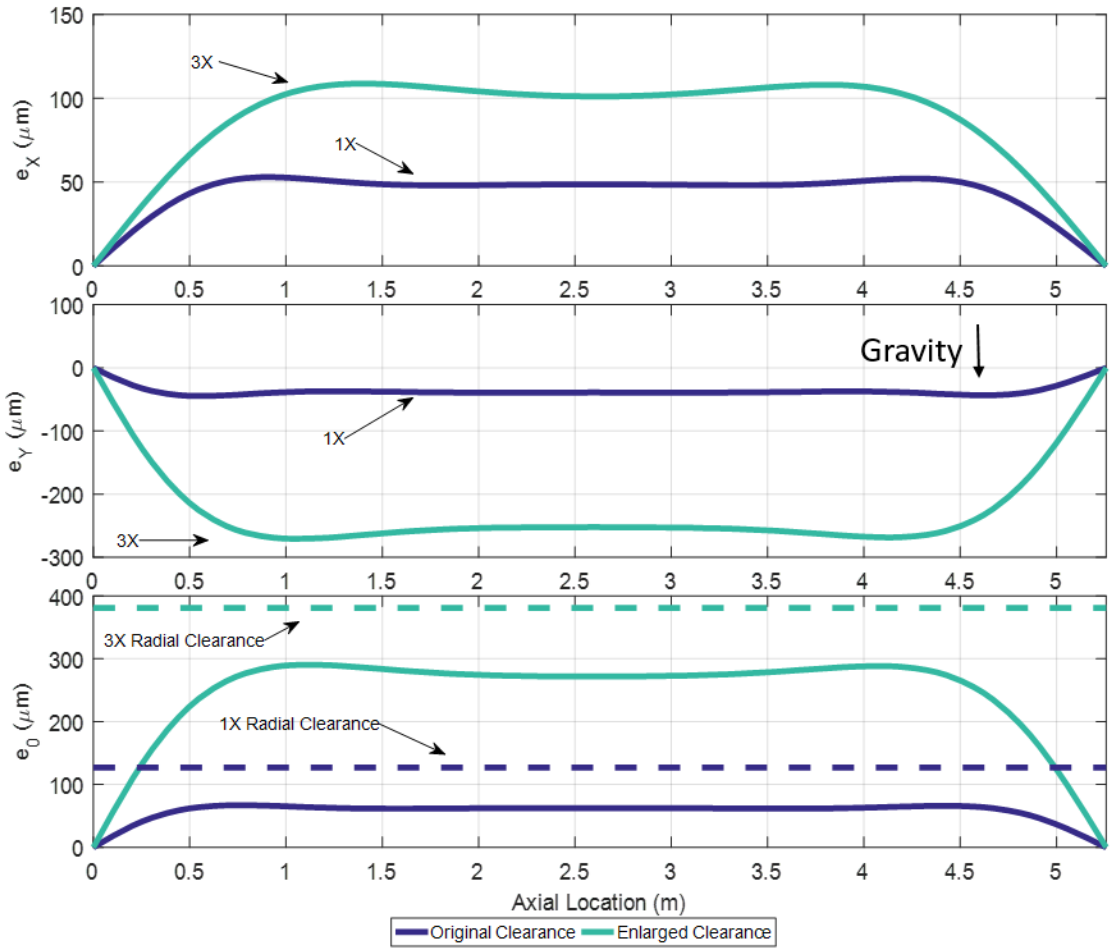

Figure 5.3: 1 cP Horizontal static position with the housing fixed at zero displacement and standard gravity.

Figure 5.4 shows the static position of the rotor for a horizontal application with a process fluid of 30 cP instead of 1 cP. The maximum displacement with the 1X 30 cP is 10.1 μm, which is lower than the 1 cP fluid. The X displacement is significantly, by a factor of 25 times, larger than the Y displacement. This indicates high cross coupled stiffness which leads to stability problems. The maximum displacement is 10 μm which gives an eccentricity ratio of 0.08 at the interstage seal. The low eccentricity ratio can lead to whirl and unstable operation even in a horizontal orientation. The 3X 30 cP case has a

maximum eccentricity of 124.4 μm. This gives an eccentricity ratio of 0.33. With the 3X 30cP, the ratio between the X displacement and Y displacement has been reduced compared to 1X 30cP. This shows slightly less coupling between the X and Y directions.

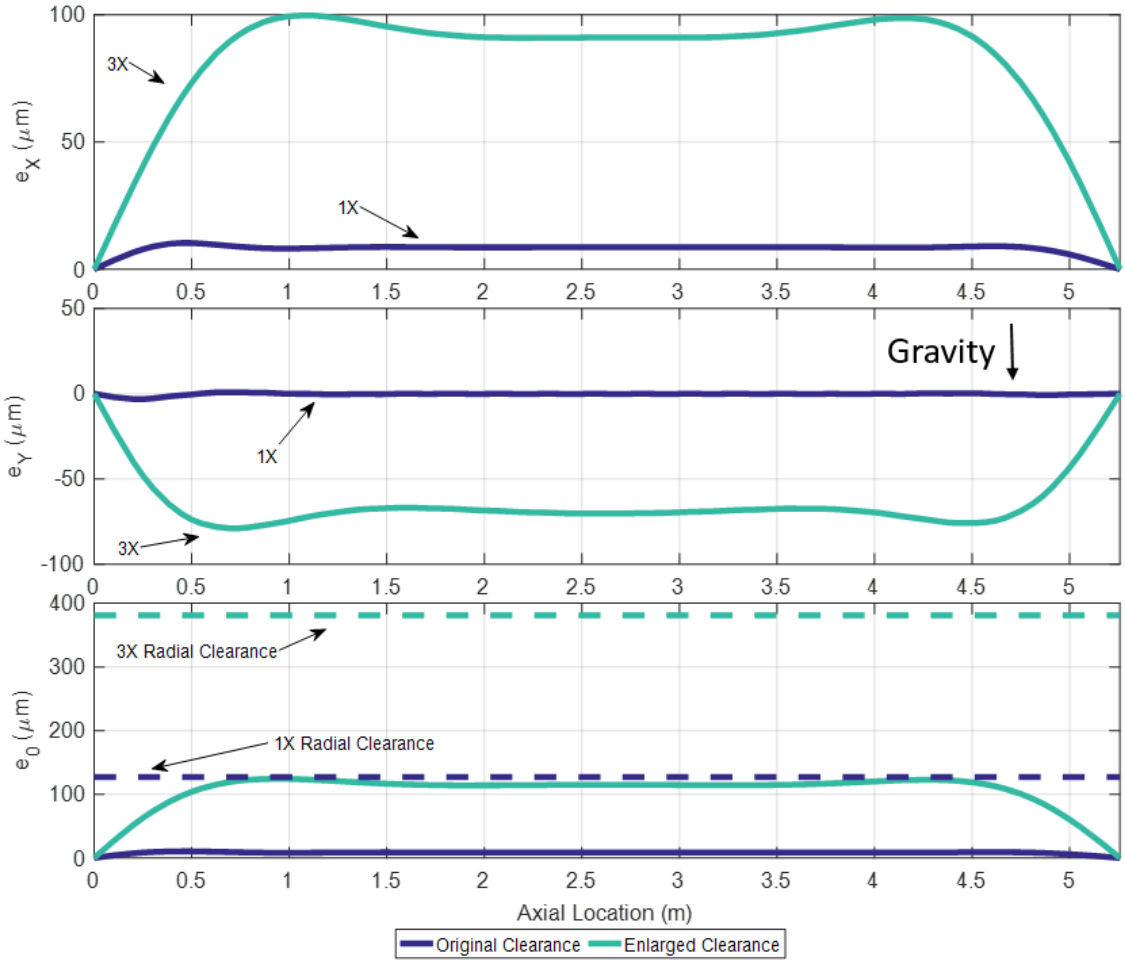

Figure 5.4: 30 cP Horizontal static position with the housing fixed at zero displacement and standard gravity.

5.3 Intermediate Support Horizontal Statics

In the past section, section 3.2, the housing is set to zero displacement for all axial positions. Surface mounted ESPs have intermediate support to hold the long housing. The intermediate support allows the housing to sag due to gravity between supports. The SEP for this section will therefore include gravity on both the rotor and housing. The supports are commonly laser aligned so for these predictions the model will be considered in line. The support spacing is chosen to be 1.04 meters based on a similar 2500 psi 600 hp surface mounted ESP.

Figure 5.5 shows the difference between a purely zero horizontal housing and a housing with intermediate stiff connections. The model is 1X 1cP. Similar trends are seen with the other 3 cases. The stiff connections are tuned in this model such that there is practically no deflection at the support locations. This comes to a support stiffness of $6 * 10^{10}$ N/m. In between the supports there is a minimal sag of only 5 μm. This amplitude depends on the stiffness of the housing and weight of the housing. The comparatively large diameter for the housing is the reason there is no significant impact from intermediate support.

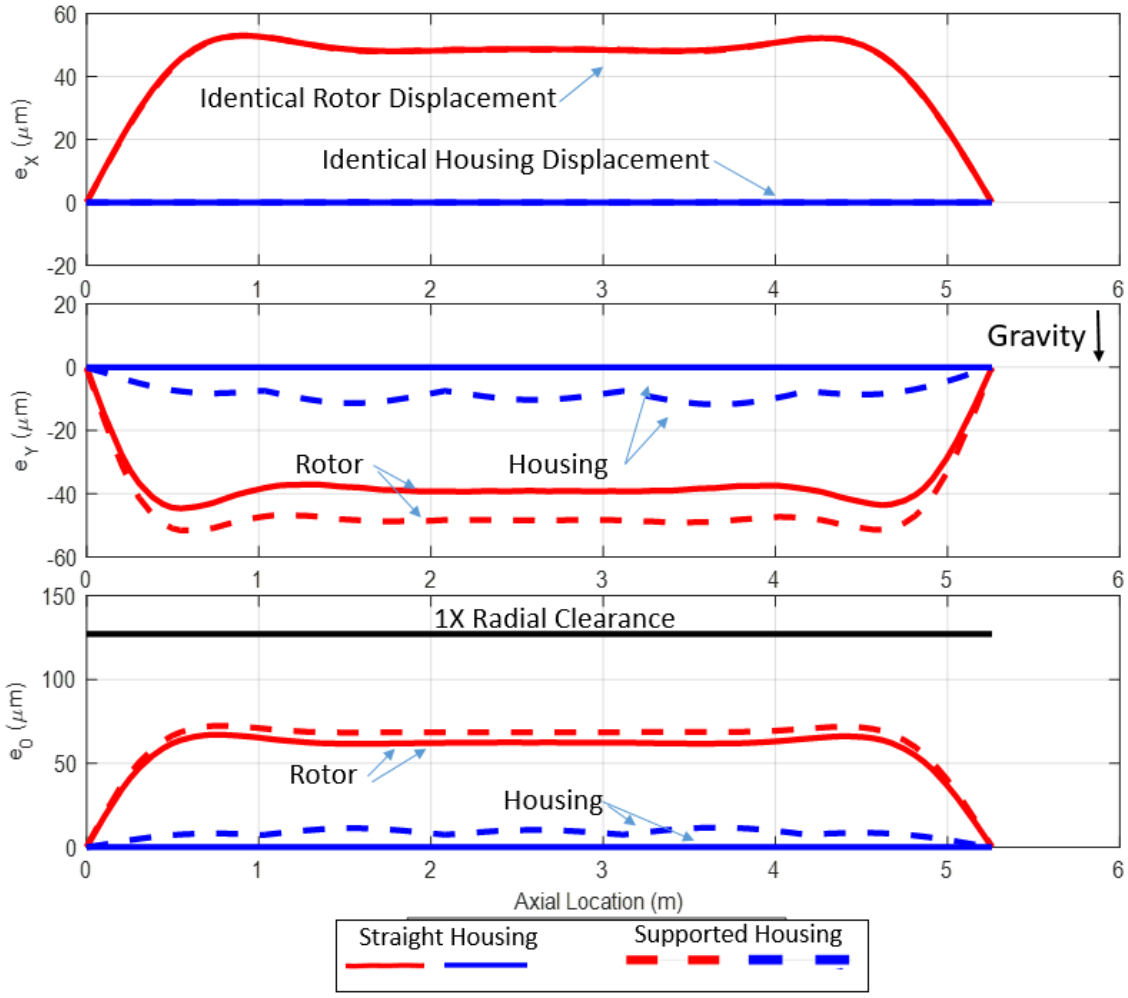

Figure 5.5: Horizontally mounted ESP with intermediate support every 1.04 meters. Model is 1X 1cP

5.4 Statics of Vertical Mounted ESP with Housing Curvature

Loading on seals in an ESP may also be from curvature. In the following predictions the 20 stage ESP model will be subjected to a curvature of the housing in the *Y-Z* plane. Figure 5.6 shows a three dimensional view of the imposed curvature on the housing. This curvature is an arc of constant radius. The rotor follows close to this shape. Figure 5.7 shows a three dimensional view of the eccentricity versus axial positon. A rotor

that follows the same path as the housing's center would be at zero in the *X* and *Y* directions. The black line indicates the path of the housing's center. The path of the housing's center follows the designated curvature. The red line is the SEP of the rotor for an ESP with 1 cP fluid and original clearances subjected to a curvature of 1 DOC. The relative static shape of the rotor is a complex shape that extends out in both the *X* and *Y* directions. The shape is fairly symmetric with respect to the symmetric input curvature.

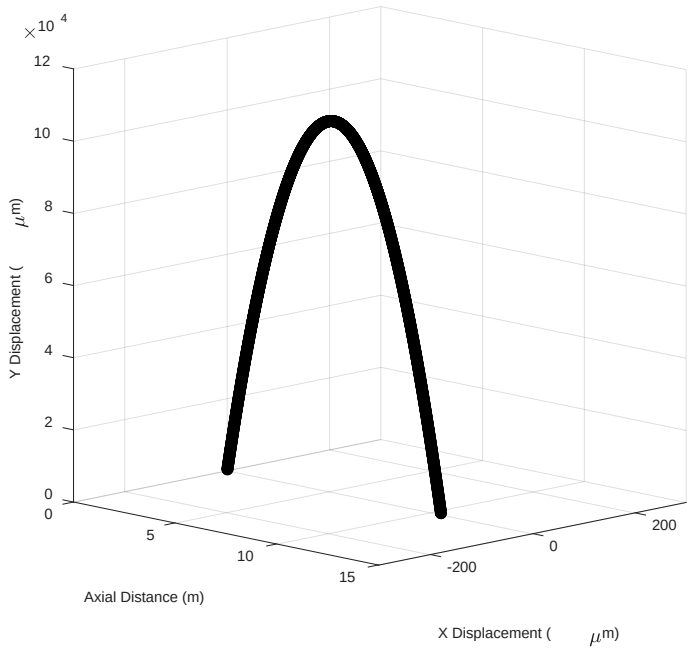

Figure 5.6: Profile of imposed curve on housing.

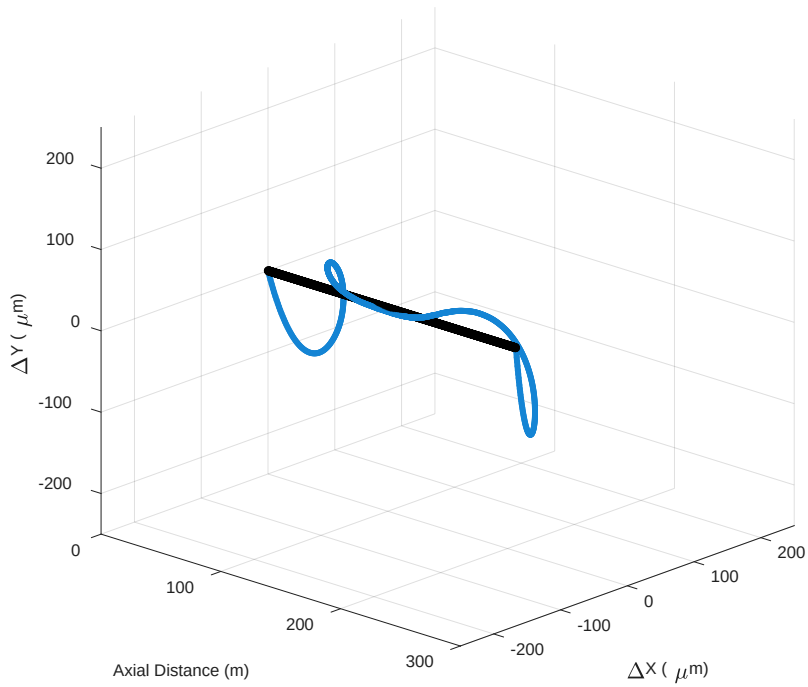

Figure 5.7: Three dimensional views of static equilibrium position in sample ESP pump section with 1X 1 cP. Red line is the relative rotor-housing lateral position. Black line is the centerline for the housing.

Figure 5.8 shows the error for the 1X 1 cP case. The graph contains four different error lines. G_{RMS} is the RMS of the vector {G} that the Newton-Raphson solver is iterating towards zero. The Ecc (ϵ_0) vector is shown as an RMS and a max value. The attitude angle (ϕ) is also shown as the RMS of the vector. All four of these values start rapidly declining at iteration 6 showing convergence on a solution. At iteration 12 the solution has got into a small enough margin of error. There is little loading in low curvature cases. The eccentricity is then close to zero for all locations. During this circumstance, the error

converges to an acceptable level. The error is from the interpolation error of the seal reaction forces at a near-zero eccentricities.

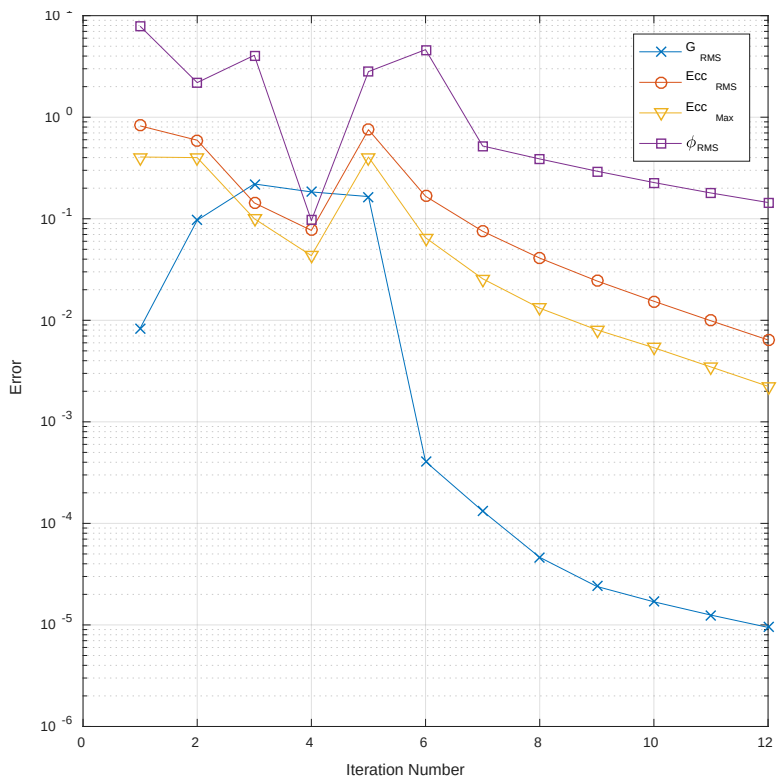

Figure 5.8: Error graph for vertical 1 cP 1X Cr. G is the vector that Newton-Raphson solves for zero. RMS is Root Mean Sum of the vector.

The three dimensional view in Figure 5.7 is broken down into its relative rotor-housing displacement components in Figure 5.9. The housing curvature is increased until a rub. e_0 is defined as the radius/magnitude of the ΔX and ΔY position vector. The e_0 magnitude is useful for showing a static rub, while the ΔX and ΔY are useful in showing the changes to the overall shape of the rotor. The profile is similar to the profile shown in Figure 4.8. No dynamics are included in this section, this is only the static equilibrium

position of the rotor. Increasing the housing curvature increases the maximum displacement between the housing center line and the rotor. For 1X 1 cP the maximum curvature before a static rub is predicted at 13 DOC. A typical curvature of the housing is around 3.5 DoC, which yields no significant eccentricities [3].

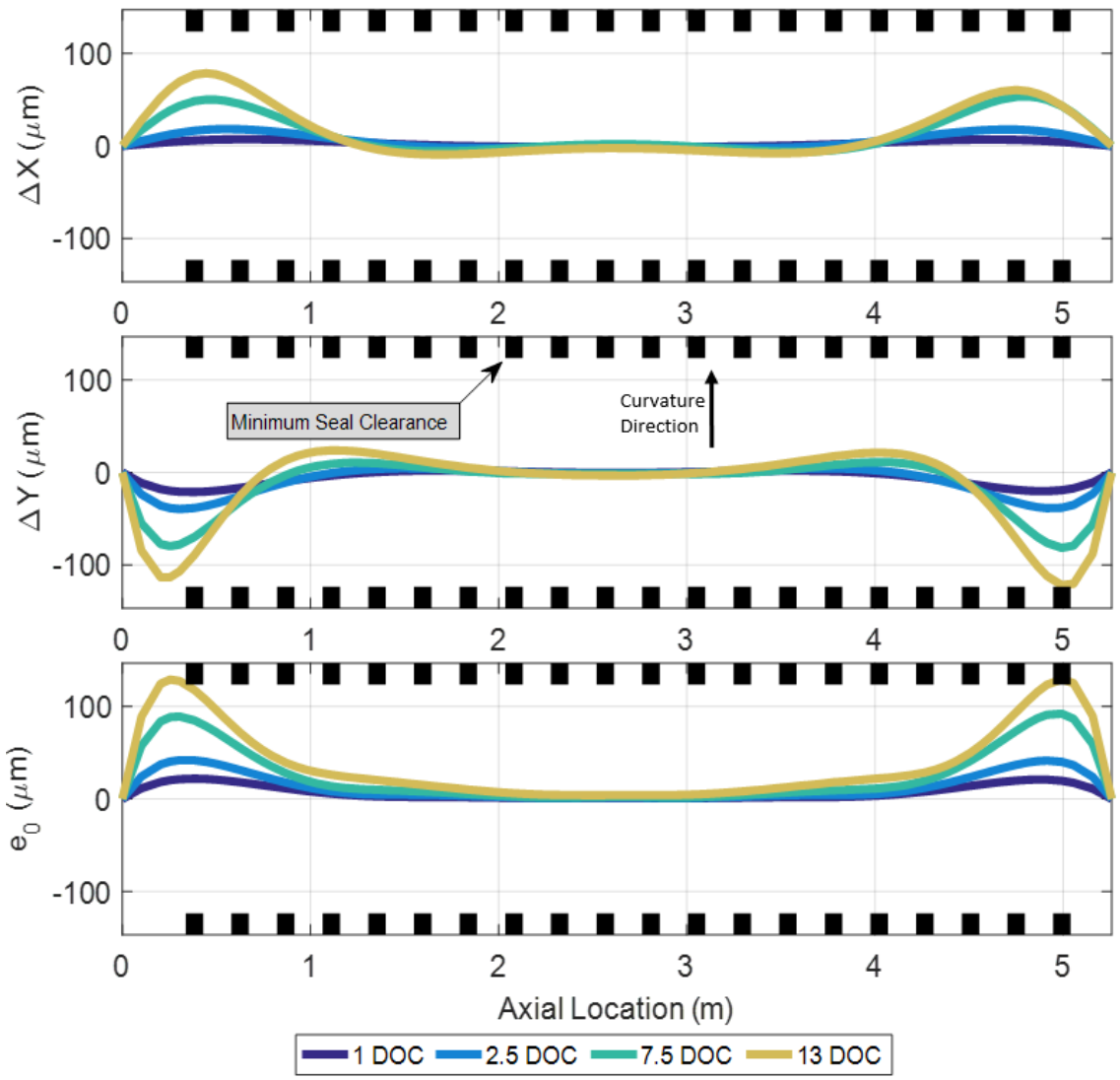

Figure 5.9: SEP from curvature in the *Y-Z* plane on vertically mounted ESP. Case 1X 1cP. Black markings are minimum radial clearance locations, which are the interstage seals. If these intersect with a line, there is contact.

To the author, this is an interesting prediction, the shape was not expected before the calculations were performed. This shape shows that only the last seal on each side moves closer to the wall and generates larger centering forces. The resulting impacts on stability and dynamics due to imposed curvature are small, because only the end seals are changing in equilibrium.

With all seals worn to 3 times their original clearance the displacement greatly increases while the maximum eccentricity for the seals are relatively unchanged. Figure 5.10 shows the new SEP for 3X 1 cP. The equilibrium position has a more gradual return to center and does not overshoot the centerline. This is from the lower stiffness of the seals.

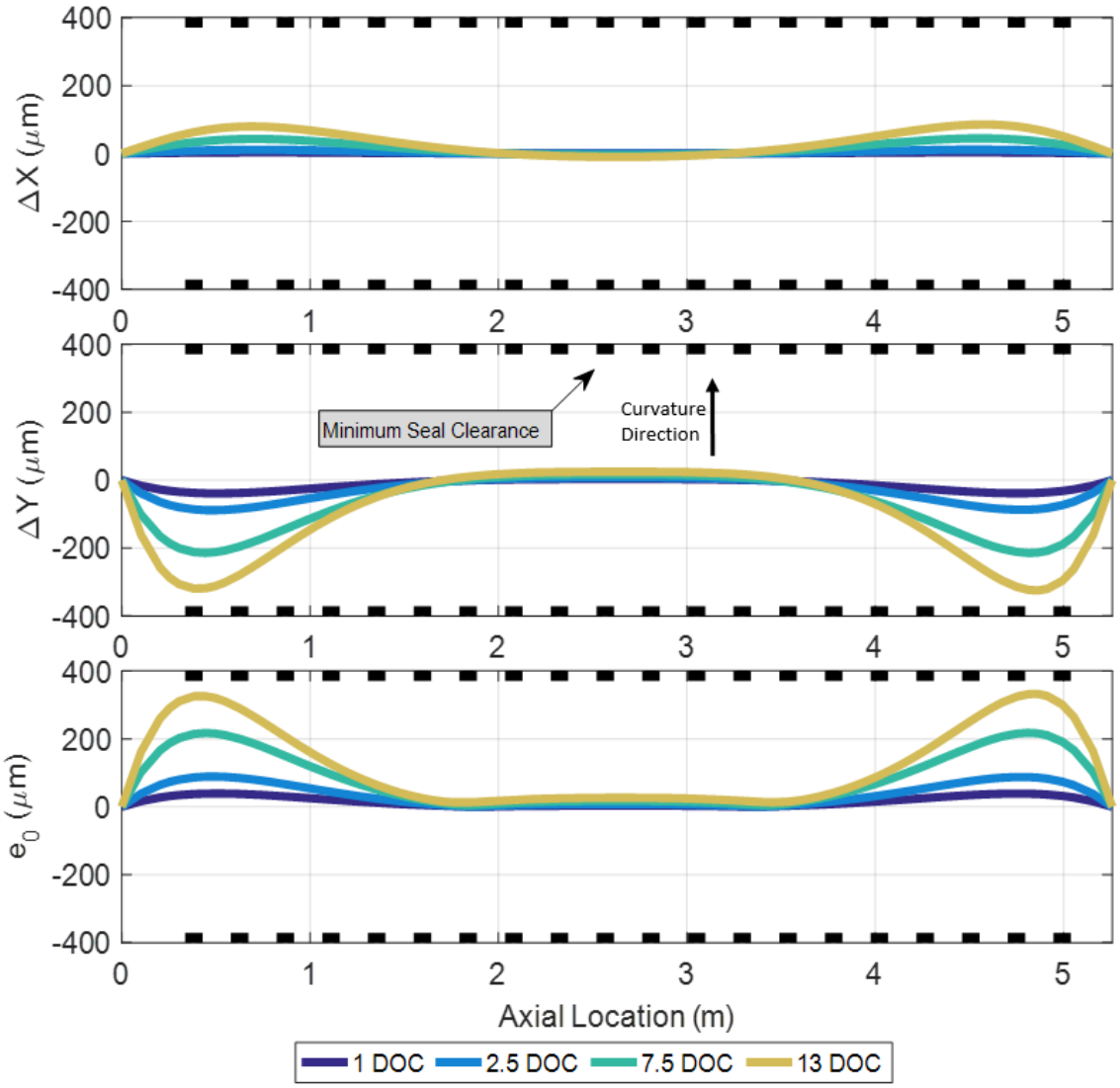

Figure 5.10: SEP from curvature in the *Y-Z* plane on vertically mounted ESP. Case 3X 1cP. Black markings are minimum radial clearance locations, which are the interstage seals. If these intersect with a line, there is contact.

Figure 5.11 shows the relative rotor-housing shape for 1X 30 cP. The SEP is close to the center for a larger portion of the shaft. The ends are the only affected zones. 30 cP as a lubricant makes the seal's stiffness approach infinite values close to the wall so no static rub is expected. Increasing the curvature only changes the eccentricity of the

boundary seals on each side of the pump causing little changes to the dynamics of the system.

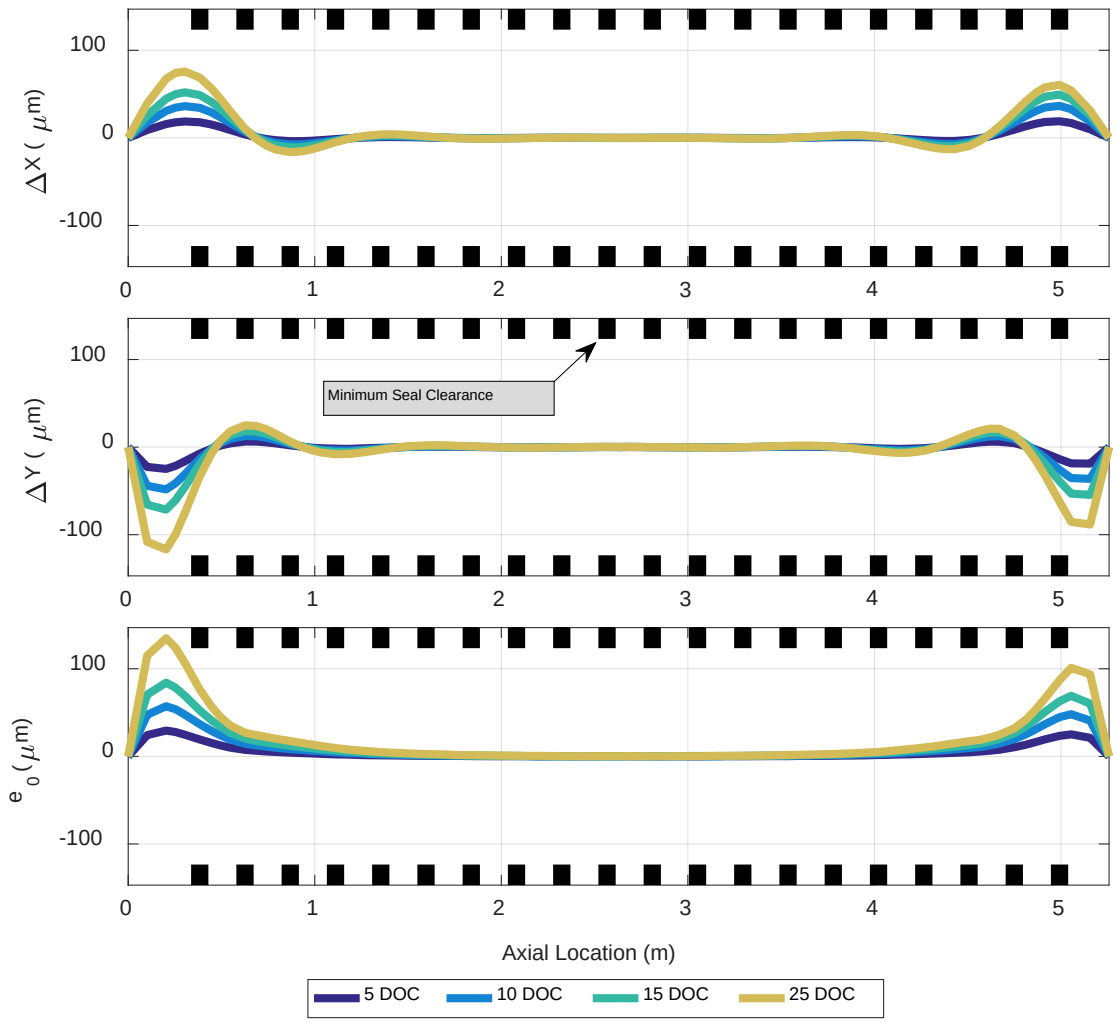

Figure 5.11: SEP from curvature in the *Y-Z* plane on vertically mounted ESP. Case 1X 30 cP. Black markings are minimum radial clearance locations, which are the interstage seals. If these intersect with a line, there is contact.

With enlarged clearances, the stiffness of the seals is reduced causing a larger portion of the shaft to be away from the housing centerline. The displacement between the shaft and housing also increases leading to the shaft being closer to the wall. For this

particular case the enlarged clearances still did not result in a rub. This trend of increasing displacement with enlarging clearances is of concern for accelerating wear conditions.

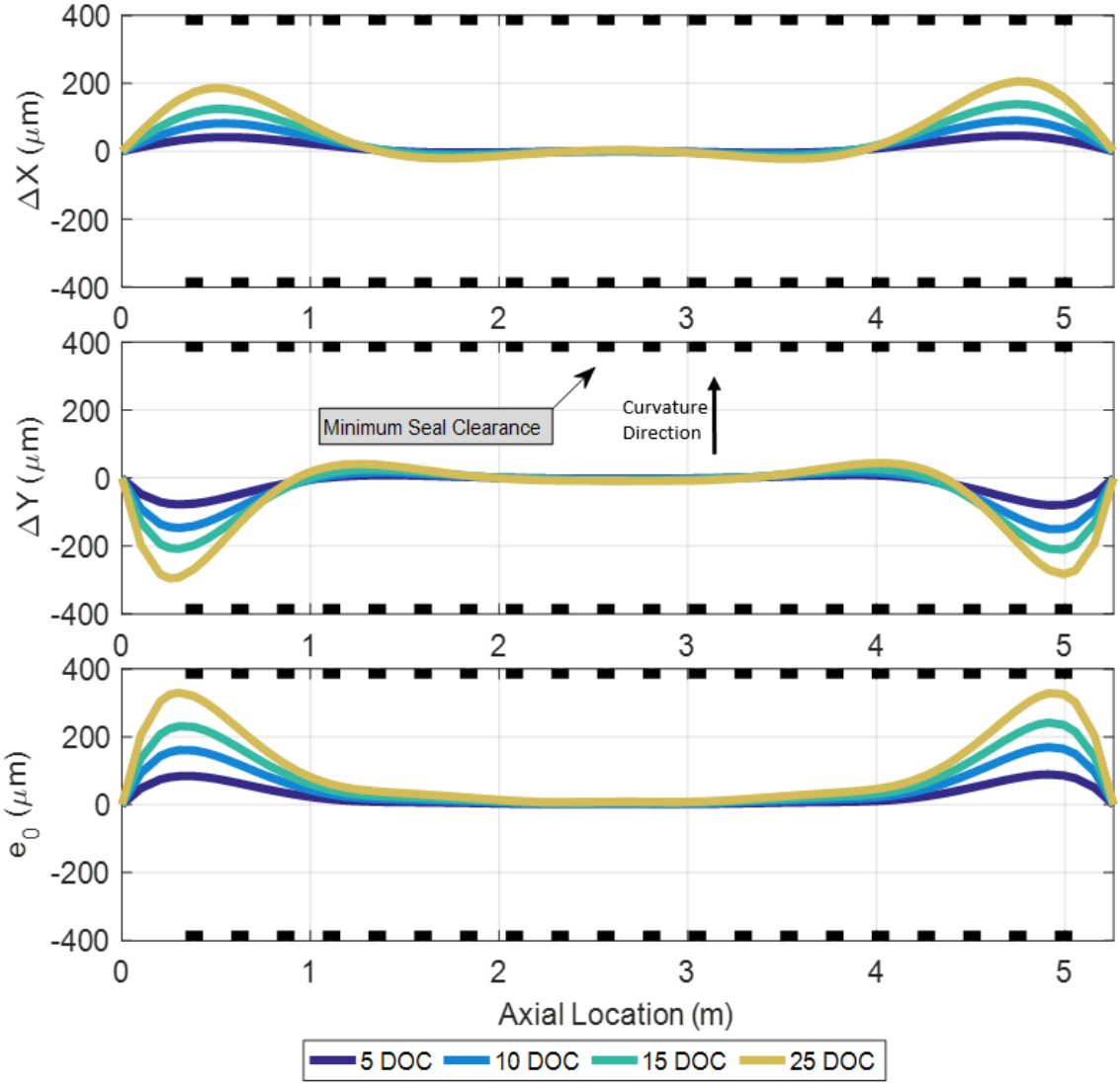

Figure 5.12: SEP from curvature in *Y-Z* plane on vertically mounted ESP. Case 3X 30 cP. Black markings are minimum radial clearance locations, which are the interstage seals. If these intersect with a line, there is contact.

5.5 Dynamic Stability about Equilibrium Position

A calculated SEP allows the seal rotordynamic coefficients to be calculated. These coefficients are used in a rotordynamic analysis of a model. In this section, stability is examined for the vertical and horizontal sample ESP. If the system is stable, dynamic response is reported to determine if a correct equilibrium position will change the dynamic response as well. The damping ratio is determined by the eigenvalues of the system using

$$\boldsymbol{\lambda} = 2\zeta\omega_n \pm j\omega_d = -2\zeta\omega_n \pm j\omega_n\sqrt{1-\zeta^2} \tag{5.1}$$

Where $\boldsymbol{\lambda}$ is the calculated eigenvalue, ω_n is the natural frequency, ω_d is the damped natural frequency, and ζ is the damping ratio.

Figure 5.13 shows the damping ratio of the first 10 modes for a system with 1X 30 cP. The damping ratio for several low-frequency modes are negative at zero curvature and stays negative as curvature increases. A system with negative damping ratios means the system is linearly unstable. An unstable system does not have a bounded linear dynamic response. 3X 30 cP exhibits the same negative low frequency modes for curvatures. Therefore, no dynamic response was calculated for 30 cP as a process fluid. Figure 5.13 also shows the damping ratios are increasing with curvature for the same modes. The curvature only has a major effect on the eccentricity of the boundary seals on the sides of the pump as shown in Figure 5.11. A curvature of 15 DOC is needed to see any changes to the stability of the system. Increasing the curvature more to 30 DOC is not enough to stabilize the overall system. For the horizontal case, both 1X 30 cP and 3X 30 cP remained linearly unstable.

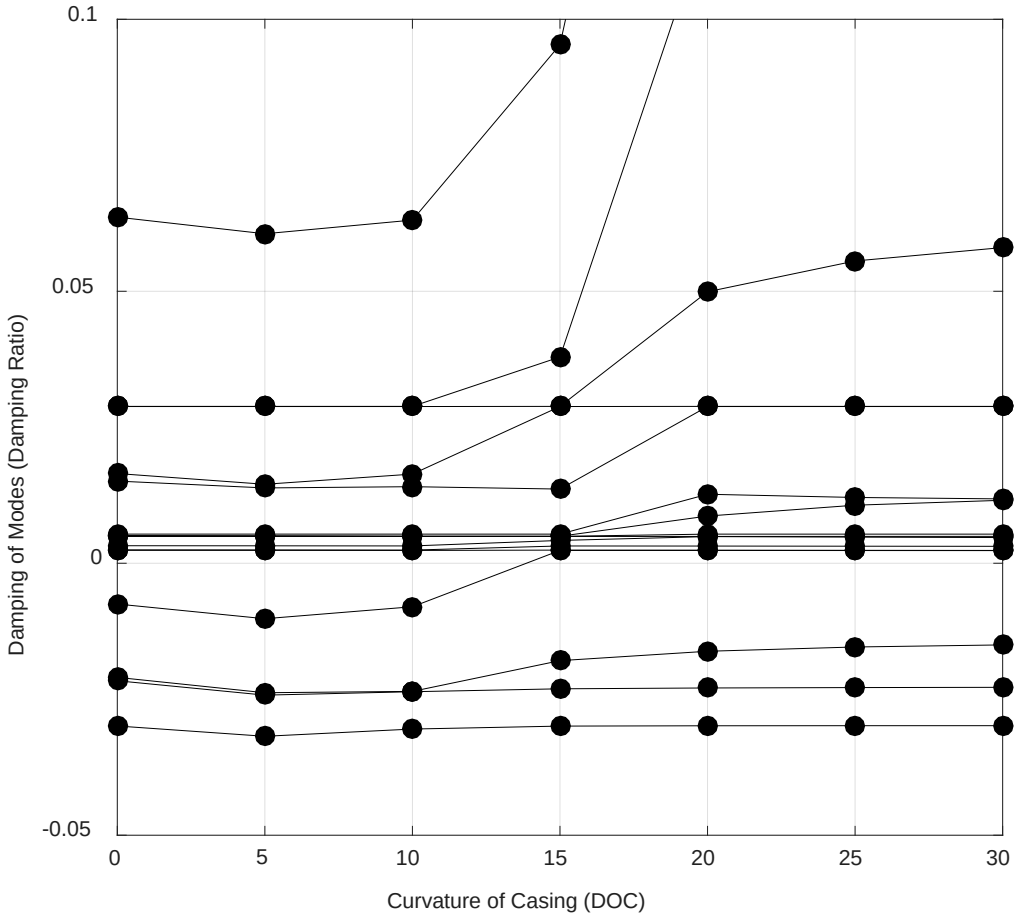

Figure 5.13: Damping ratio of sample 20 stage ESP with changes to curvature. Case 1X 30cP ω=3600 rpm

Figure 5.14 shows the damping ratio of the model with 1X 1cP. Only the lower modes close to zero are shown. The lower modes have relatively no change to damping ratio with the increase in curvature. One mode decreases with increasing curvature. The system is stable for all curvatures. 3X 1 cP exhibits similar trends. For a horizontal case with 1 cP fluid, both 1X and 3X, the system remains stable.

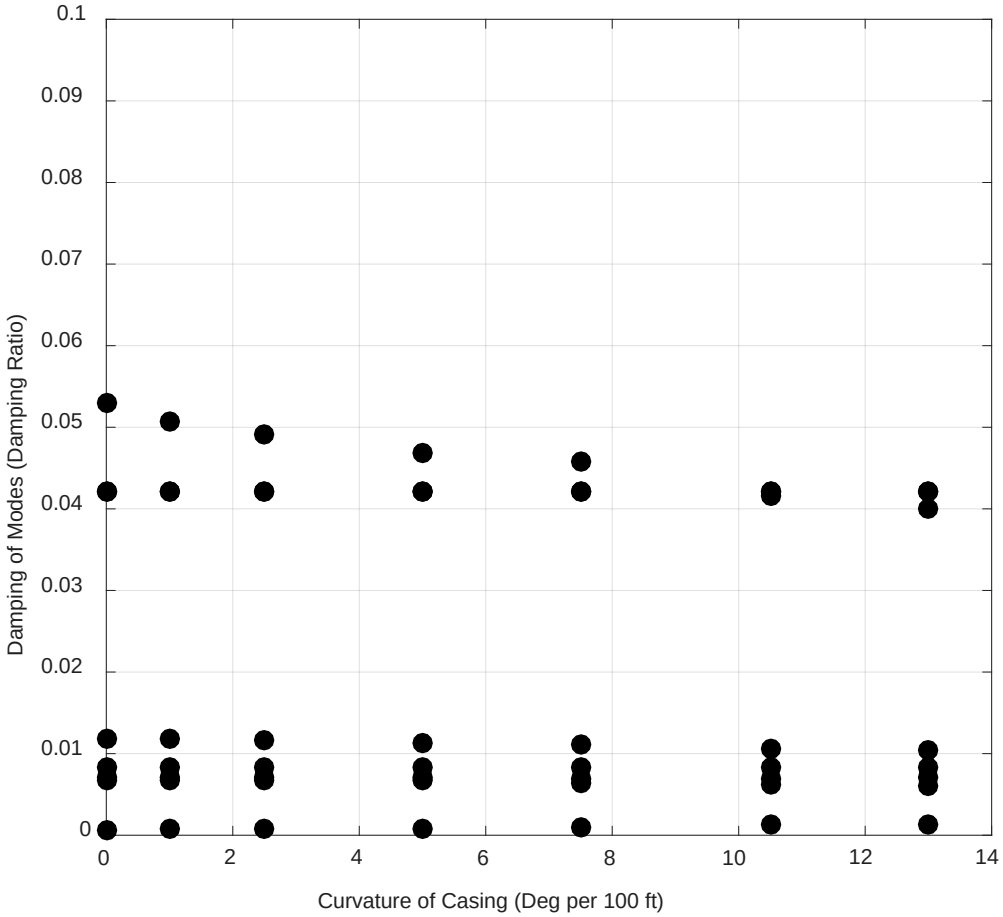

Figure 5.14: Damping ratio of sample 20 stage ESP with changes to curvature. Case 1X 1cP ω=3600 rpm 0.7 preswirl

5.6 Dynamics around Equilibrium Position

Looking at the SEP is not enough to determine a rub condition. A rotor might have a static rotor position near the wall of a seal and still rub due to vibrations. The linear dynamic response of a rotor is about its SEP. The total response is then the static position plus the dynamic response. This total response can then be used to check for a dynamic

rub. The interstage location at every stage is shown in the following graphs because these seals have the tightest clearances.

The total response is created by taking the relative rotor-housing static output and adding it to the relative rotor-housing dynamic ellipse output. The equation used to find the total *X* and total *Y* response is

$$\begin{aligned} U_{TX} &= e_X + a_{maj} * \cos(\omega t)\cos(\psi) - a_{\min} * \sin(\omega t) * \sin(\psi) \\ U_{TY} &= e_Y + a_{\mathrm{maj}} * \cos(\omega t)\sin(\psi) + a_{\min} * \sin(\omega t) * \cos(\psi) \end{aligned} \tag{5.2}$$

U_{TX} is the total dynamic response in the *X* direction, U_{TY} is the total dynamic response in the *Y* direction, ωt is plotted between 0 and 2π for the complete response. ψ is the angle of the ellipse with respect to the positive *X* axis. The coefficients a_{maj} and a_{min} are the magnitude of the major and minor axes respectively. Each blue line indicates the relative rotor-housing motion at the interstage seal. There are a total of 20 blue circles/ellipses designating each interstage location. This would be a similar view to “looking” axially in the housing at the rotor while running.

Figure 5.15 shows the total response of a horizontal ESP with 1X 1 cP seals. For the horizontal gravity loaded case. Rub is not predicted for any seals in this condition. The calculated elliptical orbit are orientated such that rub does not occur. If it not for the orientation, the major axis of the ellipse would rub. Two rotor paths that are separate from the remaining paths. These two are at the ends of the pump and have a smaller eccentricity because of the pinned boundary condition of the rotor.

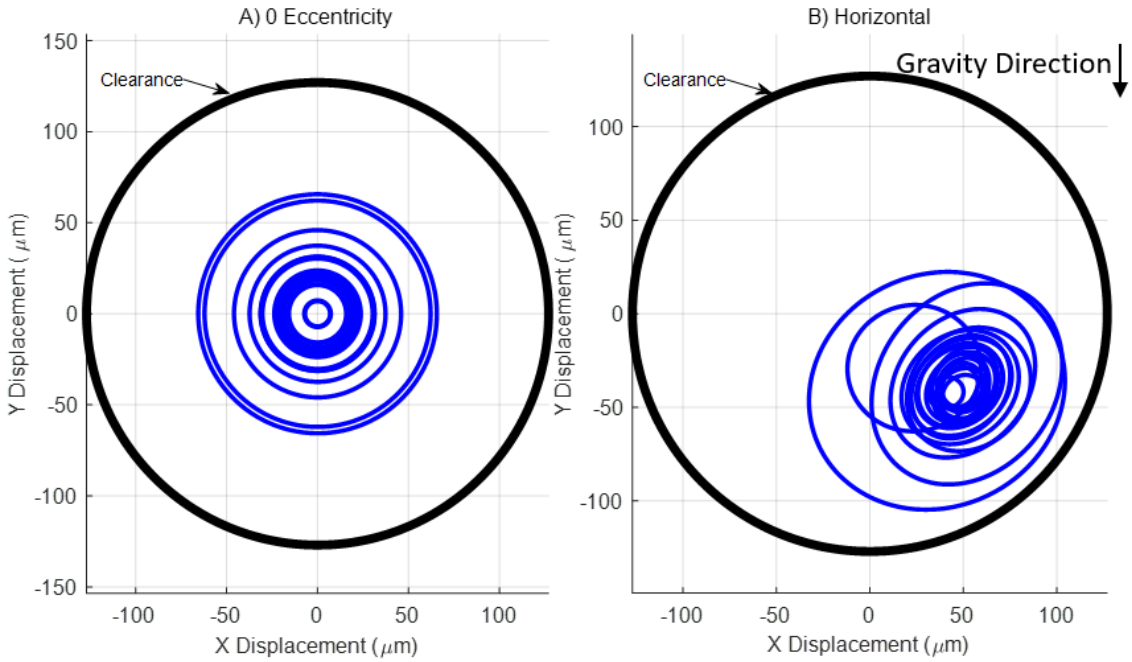

Figure 5.15: Total relative response comparison between (A) 0 eccentricity and (B) Horizontal ESP predicted about equilibrium position. Both at 1X clearances and 1 cP as the process fluid.

Figure 5.16 shows the total response, U_T, of a horizontal ESP with 3X 1 cP seals. The 3X dynamic response is small when compared to its clearance. The static position is close to the wall. No seal is predicted to rub in the 3X case. The distance between the maximum point on a path and the seal wall is 30 μm. This is close to a rub and should indicate that again, a static + dynamic case is necessary to indicate a rub or not. The dynamic response only changed minimally between the centered and loaded case.

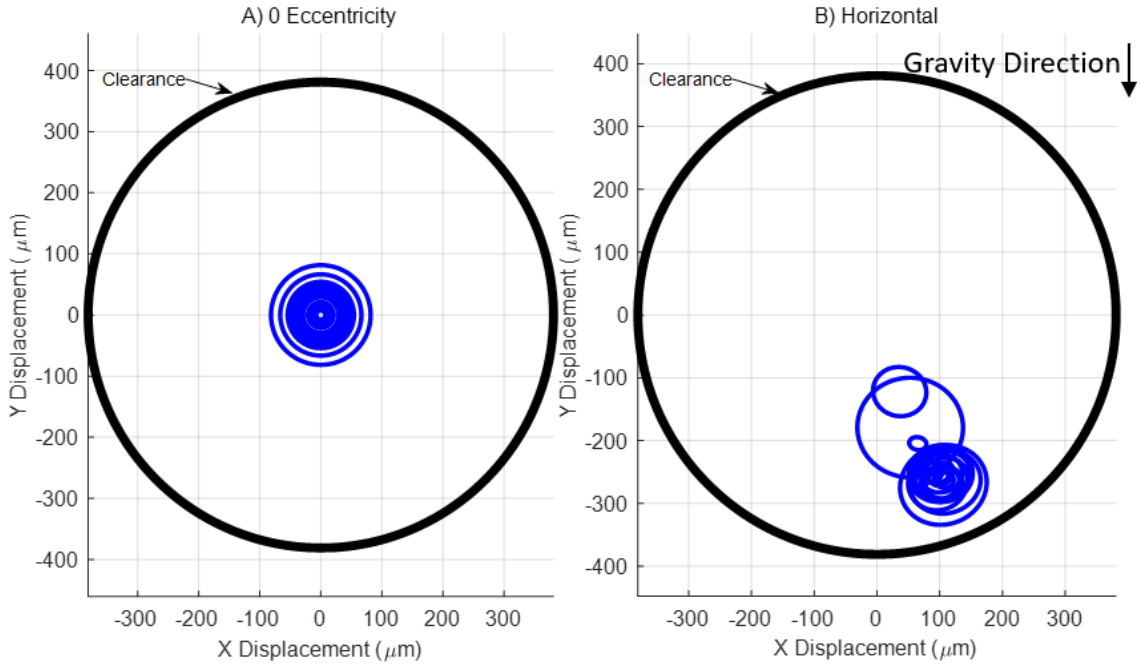

Figure 5.16: Total relative response comparison between (A) 0 eccentricity and (B) Horizontal ESP predicted equilibrium position. Both at 3X clearances and 1 cP as the process fluid.

Figure 5.17 shows the total response for 4 different cases. From top left to bottom right the DOCs are 1, 2.5, 7.5, 13 respectively. All imposed curvatures in the four graphs are in *Y-Z* plane. The 1 DOC has a similar response to the 0 eccentricity. At 2.5 DOC the end seals of the pump start to migrate towards the edge. At 7.5 DOC the dynamic response becomes highly elliptical. The seals at either end of the pump are now near the wall. Appendix E shows the max displacement for each seal along the shaft. The furthest point along the dynamic response is less than 10 μm away from the wall. The furthest response also is orientated at an angle such that dynamic response will not rub. A change in the ellipse angle will cause the possibility of a rub. In this case using the 0 eccentricity dynamic coefficients would change the resulting static+dynamic graph. At 13 DOC the

shaft is rubbing dynamically and statically. The dynamic response is not accurately portrayed here since a non-linear model including lubricated rub would need to be performed. The curvature where rub starts will be slightly less than 7.5 DOC.

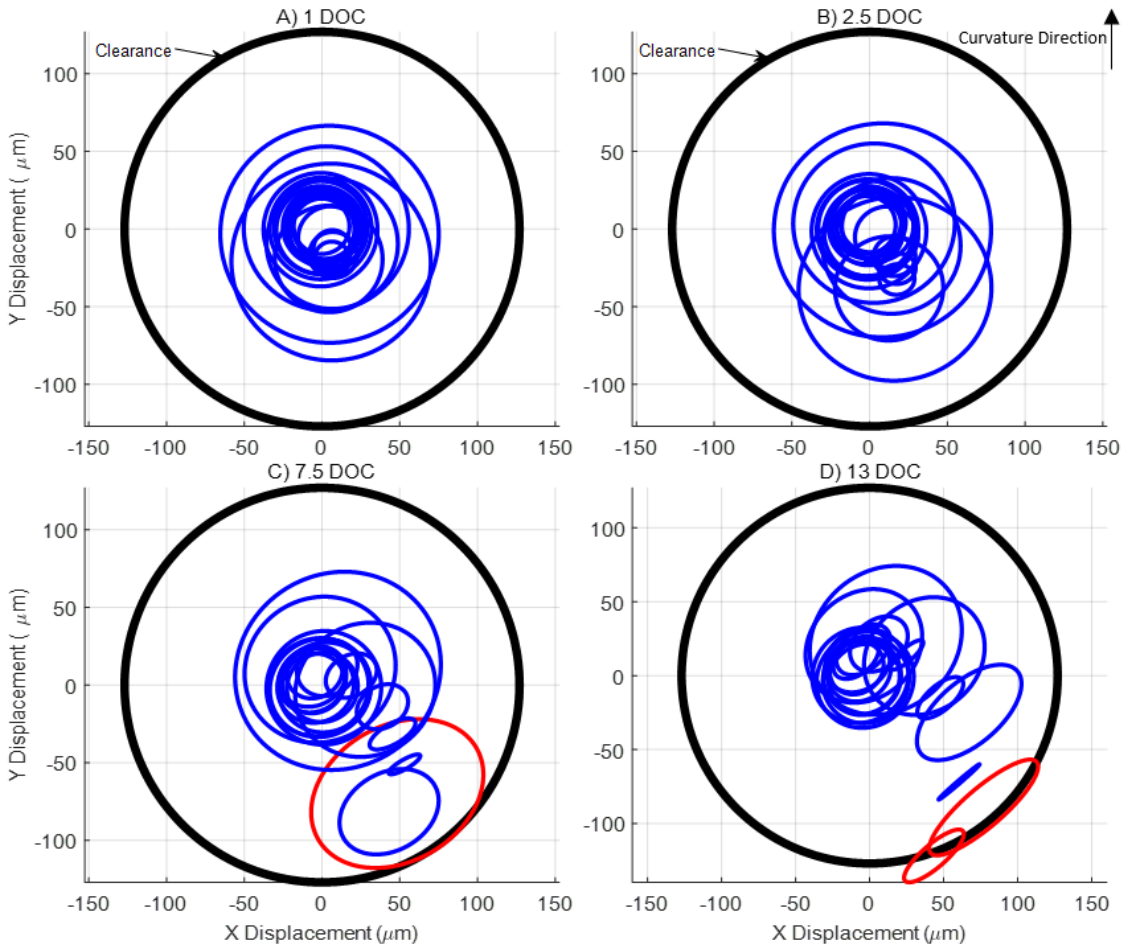

Figure 5.17: Total relative response comparison between 4 different curvatures. All at 1X clearances and 1 cP as the process fluid. Blue lines represent rotor motion. Red lines represent rotor motion contacting radial clearance.

Figure 5.18 shows the total response of a vertical ESP with 3X and water as the process fluid. The graphs again are arranged from top left to bottom right the DOCs are 1, 2.5, 7.5, 13 respectively. At 1 DOC the response is similar to the 0 eccentricity case. At

2.5 DOC there is a minor offset relative to the clearance. There is relatively no change to the system dynamics. At 7.5 DOC the displacement is nearing the wall for a few seals. The dynamics remain unchanged. At 13 DOC the dynamic orbit touches the wall. The orbit is more ellipse; however, the orbit is now not an accurate prediction since there is contact which changes the model.

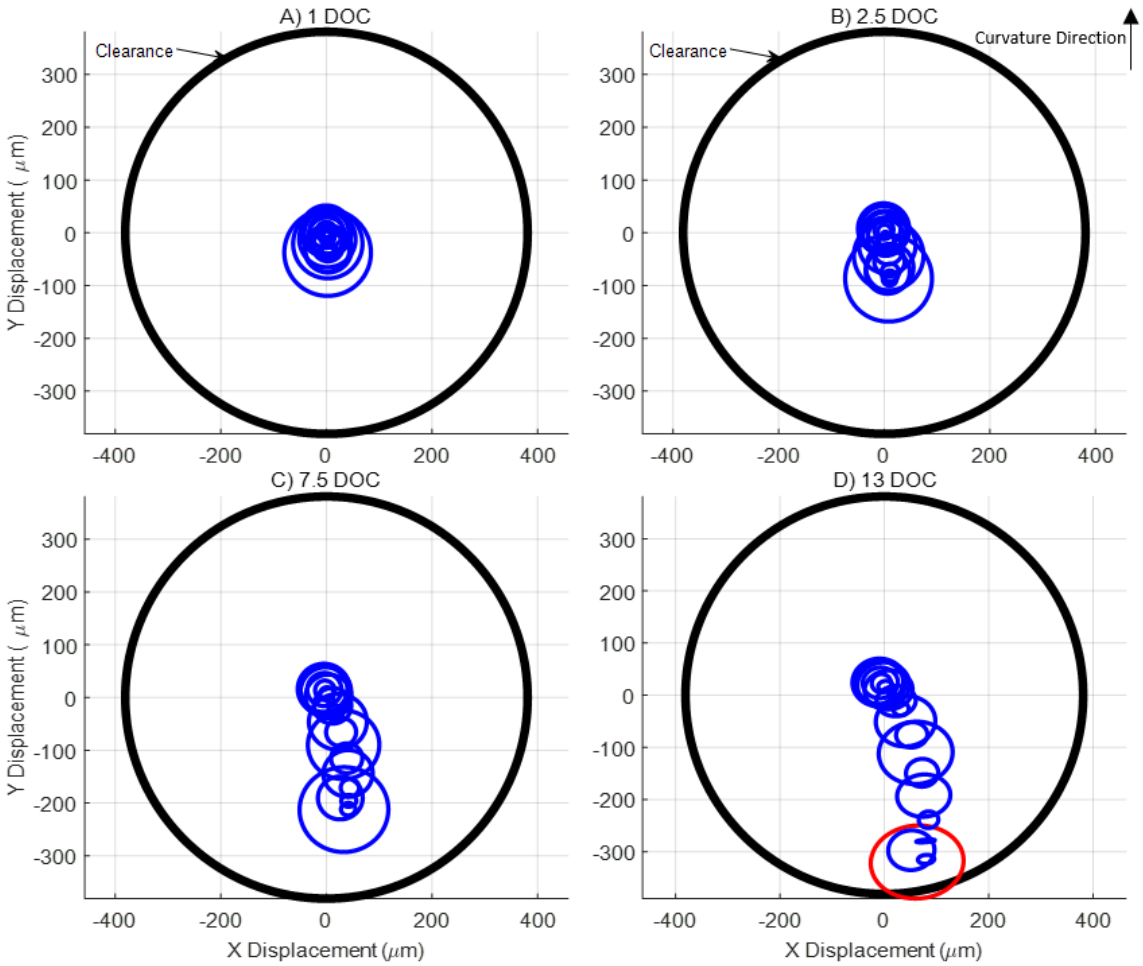

Figure 5.18: Total relative response comparison between 4 different curvatures. All at 3X clearances and 1 cP as the process fluid. Blue lines represent rotor motion. Red lines represent rotor motion contacting radial clearance.

5.7 Equilibrium Position of Vertical ESP with Helical Housing Position

The input shape of a housing can be placed in any configuration depending on the well casing shape. For two dimensional bend example, the housing is set to a helix shape with the same curvature as the one plane case. The equation for the helix is

$$\begin{aligned} X_H(z) &= c*\sin\left(\frac{2\pi \mathrm{Z}}{L}\right) \\ Y_H(z) &= c*\cos\left(\frac{2\pi \mathrm{Z}}{L}\right) - c*\cos\left(\frac{2\pi \mathrm{Z}_0}{L}\right) \end{aligned} \tag{5.3}$$

Where: c is the solved constant used to set the curvature, Z is the axial length down the housing, Z_0 is the starting axial position of the housing, and L is the length of the housing. c is found using the equations

$$\begin{aligned} d &= \frac{L}{2\pi} \\ \frac{1}{R_c} &= \frac{|c|}{c^2 + d^2} \end{aligned} \tag{5.4}$$

Where R_c is the radius of curvature. Equation (5.4) is non-linear and has 4 different values for any single R_c. The selected value for c is the lowest positive value. The lowest c gives the least X and Y displacement which yields a similar shape to an actual curved well casing.

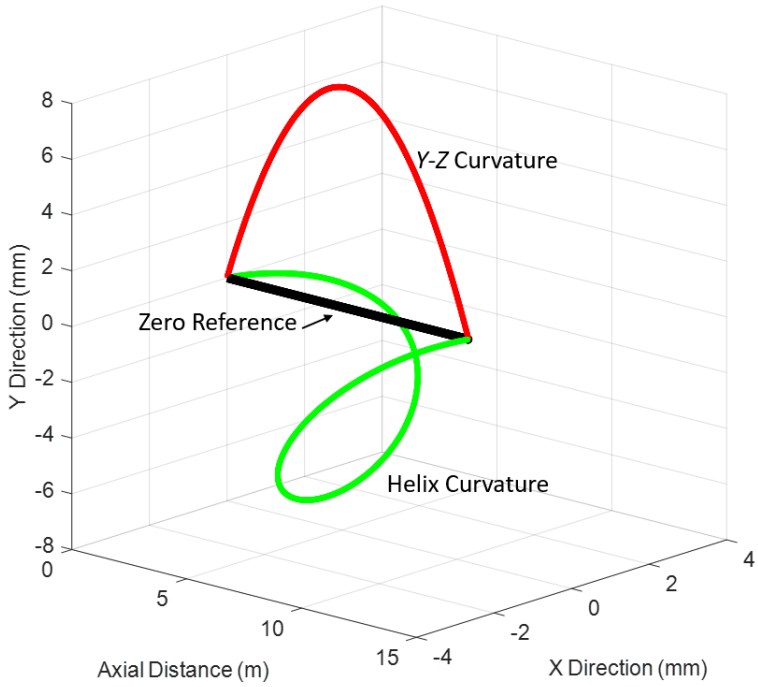

Figure 5.19: Helical housing curvature versus a *Y-Z* housing curvature.

Figure 5.20 shows the SEP of an ESP with a helix shape instead of a circular shape. The SEP is now asymmetric about the middle of the shaft. The beginning of the pump has a positive displacement away from the center. The end of the shaft has a negative displacement. The eccentricity has increased at the ends from a one plane case. This is unexpected due to the curvature for both the one plane and helix being the same. The increase in displacement may be from unequal seal forces in the *X* and *Y* plane.

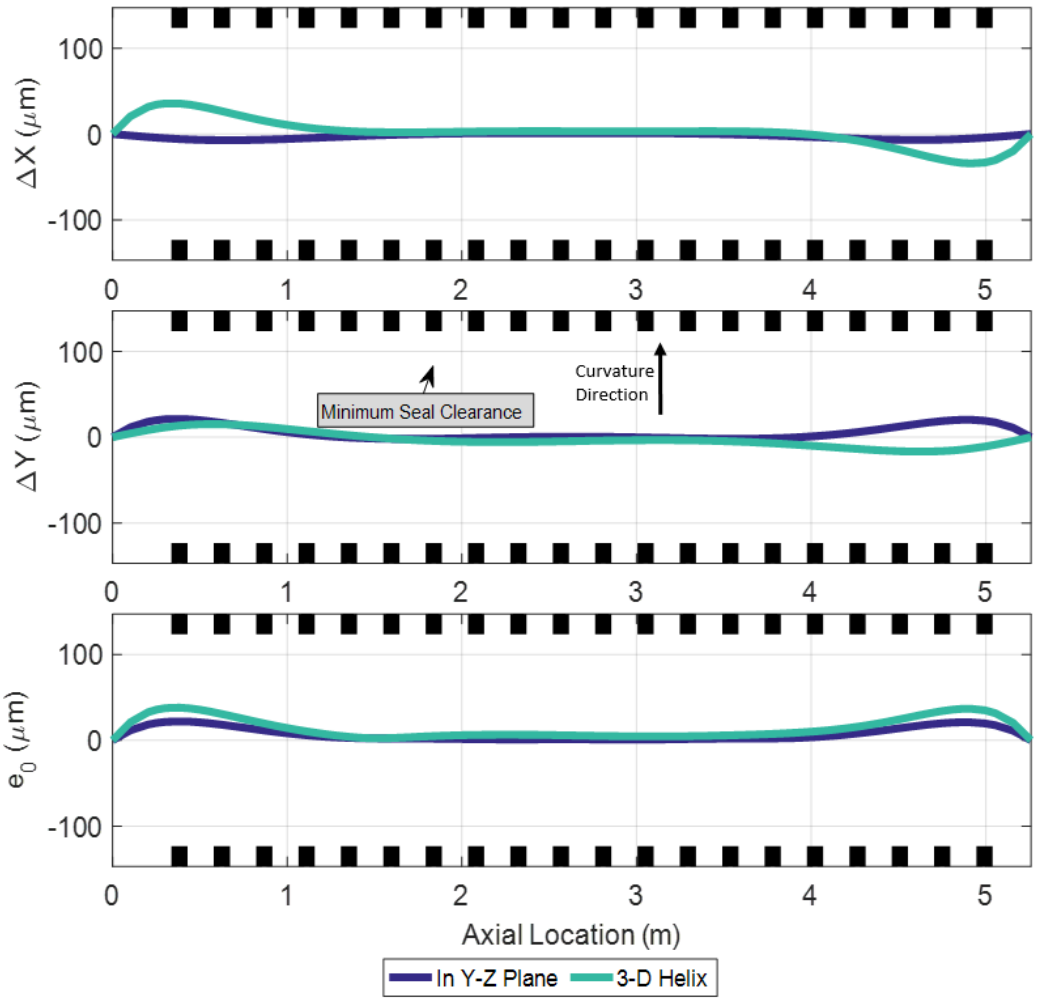

Figure 5.20: ESP with a two plane helix shape. 1 DOC and the ESP is 1X 1 cP.

6. CONCLUSION

A static equilibrium position analysis suitable for Electric Submersible Pumps (ESPs) has been developed. In addition to the rotor, it includes the housing and annular seals with eccentricity-dependent stiffness coefficients for more accurate modeling. Either the rotor or the housing can be set to a desired position, and the remaining stations positions can be solved for. The Newton-Raphson solver is accelerated by only solving for the eccentricity-dependent stations, following the analysis of Hu et al. [23]. The remaining stations are then solved for directly.

Predictions for a Baker Hughes G400 pump are shown. The predictions are for an ESP that is (1) horizontal straight housing (2) horizontal held by intermediate supports (3) vertical with an imposed curvature (4) vertical with a 3d housing profile. All 4 examples are run at viscosities of 1 cP and 30 cP to simulate turbulent and laminar flow. All 4 cases are also varied with clearance with original clearances and enlarged clearances (1X), the enlarged clearances (3X) simulate a 3X clearance enlargement due to wear. Dynamic predictions around the equilibrium position are also shown for stable cases.

6.1 Predictions for Horizontal ESP

The model in a horizontal position has gravity and buoyancy imposed laterally on the shaft. The housing is first set to a fixed straight horizontal position. The horizontal statics show a moderate eccentricity of 0.53 for 1X 1cP. This moderate eccentricity is not expected to rub with included dynamic and static response. With 1X 1cP the eccentricity

is increased to 0.76. Rub is not predicted for enlarged clearances. For analysis on ESPs, the worn condition should be checked to account for the increasing eccentricity.

With 3X 30 cP the peak eccentricity is 0.08, which is small. The static displacement is mainly in the *X* direction due to high cross coupled forces. With 3X 30 cP, the eccentricity increases to 0.33. Similar to the 1 cP case, this indicates an increase in static displacement with enlarging clearances.

Intermediate support along the length of the housing yields relatively no change from keeping the housing fixed in a straight orientation. Overall, the horizontal static position had low eccentricities that are not expected to rub. Due to the small eccentricities, there are only minor changes to the stability and response from a centered case.

6.2 Predictions for a Vertical ESP with Imposed Curvature

Predictions for a vertical orientation of the same model are also presented. The curvature of the housing is varied until rub, or close to wall rub, is expected. The curvature needed for a rub with 1X 1 cP fluid is 7.5 Degrees of Curvature (DOC). This is above a typical well curvature of 3.5 DOC [3]. The rotor's curvature shape is found to only deviate from the centerline of the housing at its ends. Hence, only a few seals to experience any eccentricity change, which results in minor changes to the rotordynamics. The 3X 1 cP is presented and shown to decrease in overall amplitude while having more seals at higher eccentricities.

A vertical orientation with 30 cP as the viscosity with the same model is presented. The higher viscosity is shown to produce a smaller length of shaft that deviates from the

housing centerline's position. The maximum curvature for a static rub with 30 cP is greater than 25 DOC. The 30 cP case is unstable for both original and enlarged clearances. No dynamic data are shown for 30 cP since the model is unstable.

The stability of the vertical ESP system for 1 cP cases is also shown. The impact of changing curvature is studied and shown to have little impact on the stability for both 1X and 3X. The stability minimally changes due to the limited number of seals that experience a change in eccentricity from curvature loading. Only the seals near the end of the rotor experience higher eccentricity ratios.

6.3 Static Predictions with a Vertical 3-D Curve Profile

The static position for a helix shaped housing at 1 cP viscosity case is lastly presented. This shape could be more realistic to an actual well casings profile. The helix static shape differed modestly in symmetry and amplitude to the one plane curvature predictions.

6.4 Future Work

- The range of seal geometries should be expanded to include non-axis-symmetric seals. These include pressure dam seals and lobed seals. This expansion would slow the solution process down since an e_0 and ϕ interpolation would be needed.
- Manufacturing probability error should be added. There are probabilities of offsets of each stages seals during assembly of ESPs. These can cause initial loading that is not considered here.

- Comparisons of this code and an experimental test rig should be completed. There is currently no data available on the effects on the statics and rotordynamics from a curved housing. A time-transient response could also be performed for comparisons.
- Forsberg [15] presented synchronous results from accelerometers mounted on an ESP housing. Full spectral results showing possible subsynchronous response would be helpful in determining stability predictions.
- A case study with real well conditions should be performed. The predictions presented in this work are good for trends; however, they do not tell the story of a particular well. A particular well will have certain contact points and a non-constant curvature that can lead to interesting results.

REFERENCES

1. Economides, M., Hill, A., Ehlig-Economides, C., Zhu, D. (2013) "Petroleum Production Systems" *Prentice Hall*

2. Caridad, J. "Electrical Submersible Pumps" Accessed June 15, 2016 http://petrowiki.org/Electrical_submersible_pumps

3. Sharma, N., McDonald, M., Mohammed, J, Daire, B., Eicks, T., Jew, L. (2209) "Optimizing Directional Drilling While Minimizing the Risk of Well Collision in Offshore Drilling" *SPE International Annual Technical Conference and Exhibition* October 4-7, 2009

4. C-fer Technologies "ESP Design & Assement for Devieated Wells" Accessed July 5, 2016 http://www.cfertech.com/how-we-help/optimize-operations/esp-design-assessment-deviated-wells

5. Radke, C. "ESP Reliability in High Curvature Wellbore JIP" Accessed July 10, 2016 http://www.cfertech.com/sites/cfertech.com/files/nodefiles/701/esp-high-curvature-wellbore-jip_0.pdf

6. Baker Hughes "Horizontal Surface Pumping Systems" Accessed July 19, 2016, http://www.bakerhughes.com/products-and-services/production/artificial-lift/horizontal-surface-pumping-systems

7. Pflueger, M. (2011), "Electrical Submersible Pump Survival Analysis" *Texas A&M University Department of Statistics Master's Thesis*

8. Durham, M. (1990), "Effect of Vibration on Electric-Submersible Pump Failures" *SPE Journal of Petroleum Technology, Vol 42 No2,* February, pp. 186-190.

9. Caridad, J. "ESP centrifugal Pump" Last Modified January 19, 2016, Accessed July 22, 2016, http://petrowiki.org/ESP_centrifugal_pump

10. Childs. D. (2013) "Turbomachinery Rotordynamics With Case Studies" Wellborn ,Texas, *Minter Spring Publishing*

11. Nelson, C. and Nguyen, D. (1988) "Analysis of Eccentric Annular Incompressible Seals: Part 1 – A New Solution Using Fast Fourier Transforms for Determining Hydrodynamic Force" *ASME Journal of Tribology, Vol 110 No 2,* April, pp. 354 – 359

12. Nelson, C. and Nguyen, D. (1988) "Analysis of Eccentric Annular Incompressible Seals: Part 2 – Effects of Eccentricity on Rotordynamic Coefficients" *ASME Journal of Tribology, Vol 110 No 2,* April, P. 361 – 366

13. Bozorgmehrian, M. (2013) "Sizing and Selection Criteria for Subea Multiphase Pumps" *University of Houston Engineering Technology Master's Thesis*

14. Al-Gheithi, S., Samanta, B., Al-Balushi, K, Al-Araimi, S., and Siddiqui, R. (2004), "Rotordynamic Analysis of an Electric Submersible Pump" *Institute of Mechanical Engineers Eighth International Conference on Vibrations in Rotating Machinery,* pp. 457-467

15. Forsberg, M. (2013), "Evaluation of ESP Vibration: Technical Process versus Black Magic," *Society of Petroleum Engineers (SPE),* ESP Workshop, Houston, TX

16. Childs, D., Norrbin, C., and Phillips, S. (2014), "A Lateral Rotordynamics Primer on Electric Submersible Pumps (ESPs) for Deep Subsea Applications" *43rd Pump and Turbomachinery Symposia*

17. Holmes, A., Ettles, C., and Mayes, I. (1978), "The Dynamics of Multi-Rotor Systems Supported on Oil Film Bearings" *ASME Journal of Mechanical Design, Vol 100 No 1,* January, pp. 157 – 164

18. Hori, Y. and R. Uematsu (1980), "Influence of Misalignment of Support Journal Bearings on Stability of a Multirotor System" *Tribology International, Vol 13 No 5,* October, P. 249-252

19. Gajan, R. (1987), "The Defelopment of a Rotordynamics Computer Code to Analyze Multi-Stage Centrifugal Pumps" *Texas A&M University Mechanical Engineering Master's Thesis*

20. Nikolajsen J., and Holmes R. (1980) "The Vibration of a Multi-Bearing Rotor" *Journal of Sound and Vibration, Vol 72 No 3,* pp. 343-350

21. Verhoeven, J. (1988) “Rotordynamic Considerations in the Design of High Speed, Multistage Centrifugal Pumps” 17th *Pump and Turbomachinery Symposia Proceedings*

22. Nikolajsen, J. (1998) “The Effect of Misalignment on Rotor Vibrations” *ASME Journal of Engineering for Gas Turbines and Power Vol 120 No 3,* P. 635-640

23. Hu, W., Feng, N, Hahn, E. (2004) “A Comparison of Techniques for Identifying the Configuration State of Statically Indeterminate Rotor Bearing Systems” *Tribology International, Vol 37 No 2,* P. 149-157

24. Miller, K. (1981) “On the Inverse of the Sum of Matrices” *MAA Mathematics Magazine, Vol 54. No 2*, P. 67-72

25. Zirkelback, N., and San Andrés, L., (1996), “Bulk-Flow Model for the Transition to Turbulence Regime in Annular Seals,” *STLE Tribology Transactions, Vol 39 No 4*, P. 835-842.

26. Salas, J., and Childs, D. (2015) “Influence of Pressure-dams in Liquid Annular Seals in the Laminar Flow Regime, Measured Results for Static and Rotordynamic Characteristics” *Texas A&M University Mechanical Engineering Master’s Thesis*

APPENDIX A. STATICS DERIVATION

Due to the limited well casing diameter, ESPs utilize a thin shell housing. In this new analysis, the added housing elements are calculated in the same manner as the structural elements in the rotor. Figure A.1 shows the numbering order for the shaft and housing. The stiffness matrix relating forces and displacements then includes the rotor and the housing. This creates a more general model and lets the program either find the position of the housing or be given a position of the housing.

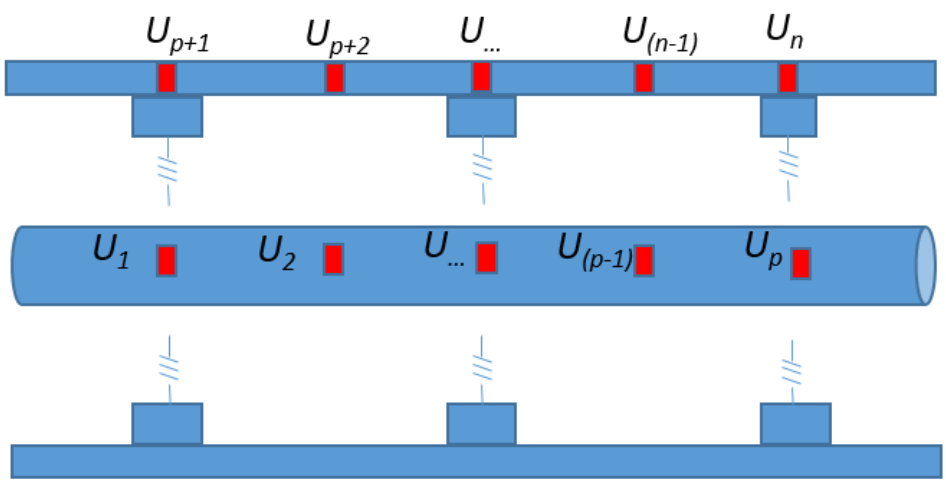

Figure A.1: Multi-line model with rotors and housings

The force and moments are also treated in the same vector, F with corresponding position and angles in a position vector, U : For example, the angular coordinates in U have corresponding moments in the F vector. Each node has 4 degrees of freedom: (1) X (2) Y (3) α which is the rotation about the x axis and (4) β which is the rotation about the

y axis. Figure A.2 shows the coordinates at every node on the model, the rotor and housing both have the same nodal degrees of freedom.

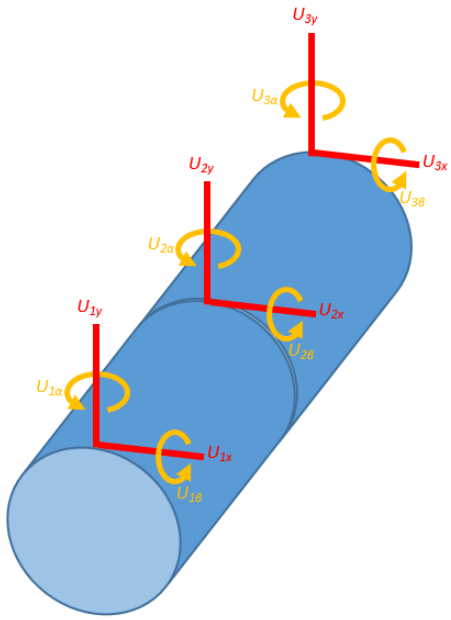

Figure A.2: Coordinate system for each node on the rotor or housing.

Each node is assembled to a position vector. This system position vector includes both the shaft and the housing. The assembled position vector includes both the *p* stations of the shaft and the *(n-p)* stations of the housing, where *n* is the number of total stations. A corresponding system stiffness matrix is assembled following the organization structure of this position vector.

The equilibrium configuration can be found by solving for when the time invarying forces and moments sum to zero for the system. The constant forces in the rotor-housing system must sum to zero to define an equilibrium configuration. This yields the equation

$$0 = \sum_{a=0}^{n} F_a \tag{A.1}$$

Where F_a is the constant force at node a in the FEM. This includes both the internal-rotor-shear forces and external-bearing-reaction forces. The moments along the FEM are

$$0 = \sum_{a=0}^{n} M_a \tag{A.2}$$

Where M_a is the constant internal and external moments at node a on the FEM. These two equations are the backbone for any statics problem. For the remaining calculations $\{F\}$ will include both the forces and moments stacked in the same vector. $\{U\}$ is defined as the vector containing the positions and angles of the rotor and housing. In this initial statics case the structural elements are assumed to have a linear stiffness. The structural elements are then taken out of $\{F\}$ and replaced with a stiffness and displacement which gives

$$[K_R]\{U_{Eq}\} = \{F_E\} \tag{A.3}$$

Where $[K_R]$ is the stiffness matrix of the structural elements. $\{U_{Eq}\}$ is the equilibrium position vector of the rotor around which the dynamic motion of the rotor occurs. $\{F_E\}$ is the external time independent force vector. In the case for finding the equilibrium position vector, $\{U_{Eq}\}$ is the unknown. The equation rearranged to solve for $\{U_{Eq}\}$ is

$$\{U_{Eq}\} = [K_R{}^{-1}]\{F_E\} \tag{A.4}$$

If the bearings have a constant stiffness throughout their eccentricity then the total static force can be split into the external static forces and linear forces as

$$\{\mathrm{F}_E\} = \{\mathrm{F}_S\} + \{F_B\} = \{\mathrm{F}_S\} + [K_B]\{U_{Eq}\} \tag{A.5}$$

Where $\{F_S\}$ is the vector containing any static force excluding linear bearings e.g. weight. $[K_B]$ is a matrix containing the bearing stiffnesses. $\{F_B\}$ is a vector containing the linear bearing forces. Equation (A.5) is then substituted into (A.4) and rearranged as

$$[K_R]\{U_{Eq}\}-[K_B]\{U_{Eq}\}=\{\mathrm{F}_S\} \tag{A.6}$$

A total linear stiffness matrix is defined as

$$[K_L]=[K_R]-[K_B] \tag{A.7}$$

Equation (A.6) then becomes

$$[K_L]\{U_{Eq}\}=\{\mathrm{F}_S\} \tag{A.8}$$

This can be solved for an exact solution of the rotor's displacement if the stiffness is constant throughout the bearing's eccentricity range. If the bearings or seals stiffnesses are eccentricity dependent, the stiffness coefficients and reaction force depend on the displacement. The displacement will then have to be solved using a Newton-Raphson solver. For the Newton-Raphson solver, the Equation (A.8) is simplified and reordered. The first step is to set the bearing force as dependent on the rotor's displacement vector at the bearing's location and take it out of the static forces. Equation (A.8) then becomes

$$[K_L]\{U_{eq}\}=\{F_s\}+\{F_{BNL}(U_{eq})\} \tag{A.9}$$

With component $\{U_{NL}\}$ being the eccentricity dependent degrees of freedom and $\{F_{BNL}(U_{eq})\}$ being the eccentricity-dependent force vector of the bearings onto the rotor. The static forces are added with the eccentricity dependent forces to create a total force vector.

$$\{F\} = \{F_s\} + \{F_{BNL}(U_{eq})\} \tag{A.10}$$

Where F is the total forces in the system. The force and displacement are split to its linear and non-linear components. The non-linear components are the stations that need to be iteratively solved for. The linear components are the stations that can be solved for analytically. [K_L] is reordered to match the new station arrangement of {U} and {F}. [K_L] is then split up into 4 submatrices that correlate to the newly split up {U} and {F}. These changes create a new equation of

$$\begin{pmatrix} [K_T] & [K_U] \\ [K_V] & [K_W] \end{pmatrix} \begin{pmatrix} \{U_{NL}\} \\ \{U_L\} \end{pmatrix} = \begin{pmatrix} \{F_{NL}(U_{NL})\} \\ \{F_L\} \end{pmatrix} \tag{A.11}$$

Where matrix [K_T] relates the non-linear displacements to the nonlinear force. Matrix [K_U] relates the linear displacements to the non-linear force. Matrix [K_V] relates the non-linear displacements to the linear force. Finally, matrix [K_W] relates the linear displacements to the linear forces.

These equations can be split up as

$$[K_T]\{U_{NL}\} + [K_U]\{U_L\} = \{F_{NL}(U_{NL})\} \tag{A.12}$$

$$[K_V]\{U_{NL}\} + [K_W]\{U_L\} = \{F_L\} \tag{A.13}$$

{U_{NL}} and {U_L} are unknown; however, since {F_{NL}} depends on the non-linear displacements, {U_{NL}} will have to be numerically solved for. Equation (A.13) can be substituted into eq. (A.12) to reduce the needed numerical analysis to one equation. First, eq. (A.13) is rewritten as

$$\{\mathrm{U}_L\} = [K_W{}^{-1}]\{F_L\} - [K_W{}^{-1}][K_V]\{U_{NL}\} \tag{A.14}$$

Which is then plugged back into eq. (A.15)to get

$$[K_T]\{U_{NL}\} + [U][K_W{}^{-1}]\{F_L\} - [K_U][K_W{}^{-1}][K_V]\{U_{NL}\} = \{F_{NL}(U_{NL})\} \tag{A.16}$$

The numerical approach used to find $\{U_{NL}\}$ is the Newton-Raphson technique. This numerical analysis iterates through a function while trying to set that function to zero. The new Equation (A.16) is rewritten with everything to the right hand side to make a new function $\{G\}$ which is

$$\{G\} = ([K_U][K_W{}^{-1}][K_V] - [K_T])\{U_{NL}\} - [K_U][K_W{}^{-1}]\{F_L\} + \{F_{NL}(U_{NL})\} \tag{A.17}$$

using substitutions of

$$\begin{aligned} [C_1] &= ([K_U][K_W{}^{-1}][K_V] - [K_T]) \\ [C_2] &= [K_U][K_W{}^{-1}] \end{aligned} \tag{A.18}$$

{G} can be simplified to

$$\{G\} = [C_1]\{U_{NL}\} - [C_2]\{F_L\} + \{F_{NL}(U_{NL})\} \tag{A.19}$$

the Jacobian of G with respect to position is

$$[J] = [C_1] + [K_B(U_{NL})] \tag{A.20}$$

Equation (A.17) and (A.20) are then used to find $\{U_{Eq}\}$. The first guess is found using equation (A.8). The non-linear bearings are set to a temporary large linear stiffness of $1\text{x}10^{12}$. This sets the rotor to center at every non-linear bearing. $\{U_{Eq}\}$ is then iteratively solved for using

$$\{U_{n+1}\} = \{U_n\} - [J^{-1}]\{G\} \tag{A.21}$$

Where $\{U_{n+1}\}$ is the guess for the following iteration and $\{U_n\}$ is the current guess. Convergence is found when G is within a small margin of 0.

APPENDIX B. GRAVITY DERIVATION

The magnitude of the total force of gravity for an object is equal to

$$F_g = m * g \tag{B.1}$$

Where F_g is the force from gravity, m is the mass, and g is the acceleration due to gravity. Figure 1 shows the weight as a uniform force, in blue, distributed along the beam. Assume the beam is pinned on either side. The weight will then cause the beam element to bend. This bend is internal between the nodes of the FEM. This bending force is then represented as an equivalent moment at each nodal location. The equivalent moment is found by the integration of the shape function over the finite element. Assuming uniform mass along the finite element, the overall model for a uniform acceleration on a beam can be expressed as a force through equation (B.1). Nodal equivalent forces then can be expressed in the same manner as a distributed force.

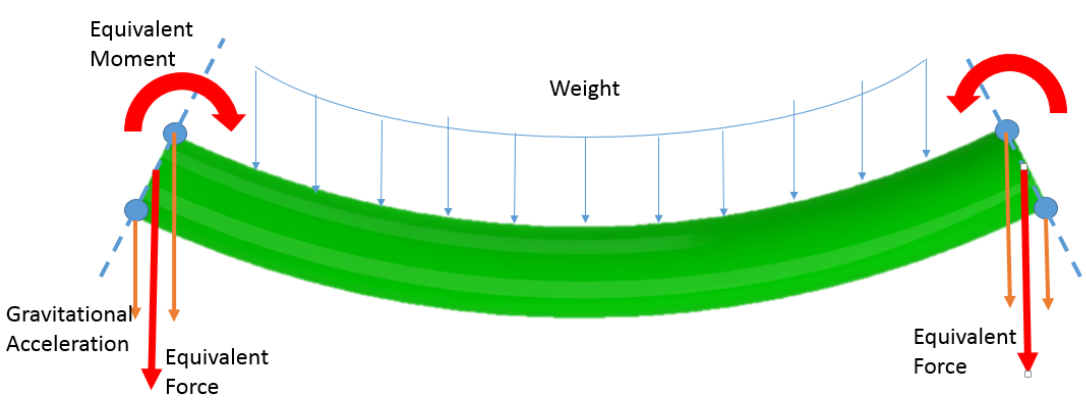

Figure B.3: Finite Element with uniform loading between nodes

For a coordinate system of

$$\begin{pmatrix} v(0) \\ \theta(0) \\ v(\mathrm{L}) \\ \theta(\mathrm{L}) \end{pmatrix} \tag{B.2}$$

Where $v(0)$ is the position at the left hand side of the finite element, $\theta(0)$ is the left hand side rotation, and both $v(\mathrm{L})$ and $\theta(\mathrm{L})$ are for the opposite side of the element ate at length L. The nodal equivalent force is

$$\begin{pmatrix} F_0 \\ M_0 \\ F_L \\ M_L \end{pmatrix} = \begin{pmatrix} \frac{mgL}{2} \\ \frac{mgL^2}{12} \\ \frac{mgL}{2} \\ -\frac{mgL^2}{12} \end{pmatrix} \tag{B.3}$$

Where F_0, M_0, F_L, M_L are the forces and moments on each side of the element. This can then be used to create a system force vector due to uniform gravity.

APPENDIX C. SEAL DATA FOR CODE VALIDATION

Table C.1: Stiffness with respect to eccentricity for validation model. Running speed of 3600rpm.

ECC	Kxx	Kxy	Kyx	Kyy
-	**N/m**	**N/m**	**N/m**	**N/m**
0.0	7.15E+05	4.84E+05	-4.84E+05	7.15E+05
0.1	7.15E+05	4.88E+05	-4.85E+05	7.15E+05
0.2	7.14E+05	5.01E+05	-4.88E+05	7.13E+05
0.3	7.13E+05	5.24E+05	-4.94E+05	7.09E+05
0.4	7.06E+05	5.77E+05	-5.11E+05	6.07E+05
0.5	6.75E+05	6.64E+05	-5.58E+05	5.14E+05
0.6	6.63E+05	7.47E+05	-6.29E+05	6.38E+05
0.7	6.73E+05	9.41E+05	-6.67E+05	8.39E+05
0.8	6.88E+05	1.48E+06	-6.12E+05	6.45E+05
0.9	6.69E+05	4.44E+06	-8.76E+05	3.12E+05

Table C.2: Damping with respect to eccentricity for validation model. Running speed of 3600rpm.

ECC	Cxx	Cxy	Cyx	Cyy
-	N-S/M	N-S/M	N-S/M	N-S/M
0.0	2.65E+03	4.37E+02	-4.37E+02	2.65E+03
0.1	2.65E+03	4.40E+02	-4.36E+02	2.67E+03
0.2	2.67E+03	4.53E+02	-4.35E+02	2.74E+03
0.3	2.71E+03	4.75E+02	-4.32E+02	2.86E+03
0.4	2.77E+03	4.95E+02	-4.28E+02	3.20E+03
0.5	2.92E+03	5.20E+02	-4.36E+02	3.81E+03
0.6	3.10E+03	5.93E+02	-4.43E+02	4.45E+03
0.7	3.30E+03	7.37E+02	-4.32E+02	5.23E+03
0.8	3.59E+03	9.39E+02	-4.16E+02	7.39E+03
0.9	4.55E+03	1.39E+03	-4.01E+02	2.52E+04

Table C.3: Virtual mass with respect to eccentricity for validation model. Running speed of 3600rpm.

ECC	Mxx	Mxy	Myx	Myy
-	N-S**2/M	N-S**2/M	N-S**2/M	N-S**2/M
0.0	1.18E+00	-7.59E-02	7.64E-02	1.18E+00

0.1	1.18E+00	-7.64E-02	7.53E-02	1.19E+00
0.2	1.19E+00	-7.84E-02	7.27E-02	1.21E+00
0.3	1.21E+00	-8.17E-02	6.81E-02	1.25E+00
0.4	1.23E+00	-7.40E-02	6.01E-02	1.28E+00
0.5	1.26E+00	-6.10E-02	5.35E-02	1.36E+00
0.6	1.30E+00	-6.75E-02	4.34E-02	1.53E+00
0.7	1.38E+00	-9.09E-02	3.26E-02	1.80E+00
0.8	1.49E+00	-1.00E-01	2.12E-02	2.20E+00
0.9	1.46E+00	-7.23E-02	5.45E-02	3.31E+00

Table C.4: Force with respect to eccentricity for validation model. Running speed of 3600rpm.

ECC	**Fx**	**Fy**
-	N	N
0.0	2.64E-02	6.33E-02
0.1	8.33E+00	1.31E+01
0.2	1.80E+01	2.71E+01
0.3	2.78E+01	4.07E+01
0.4	3.82E+01	5.37E+01
0.5	5.01E+01	6.36E+01
0.6	6.33E+01	7.25E+01
0.7	7.79E+01	8.46E+01
0.8	9.68E+01	9.84E+01
0.9	1.40E+02	1.08E+02

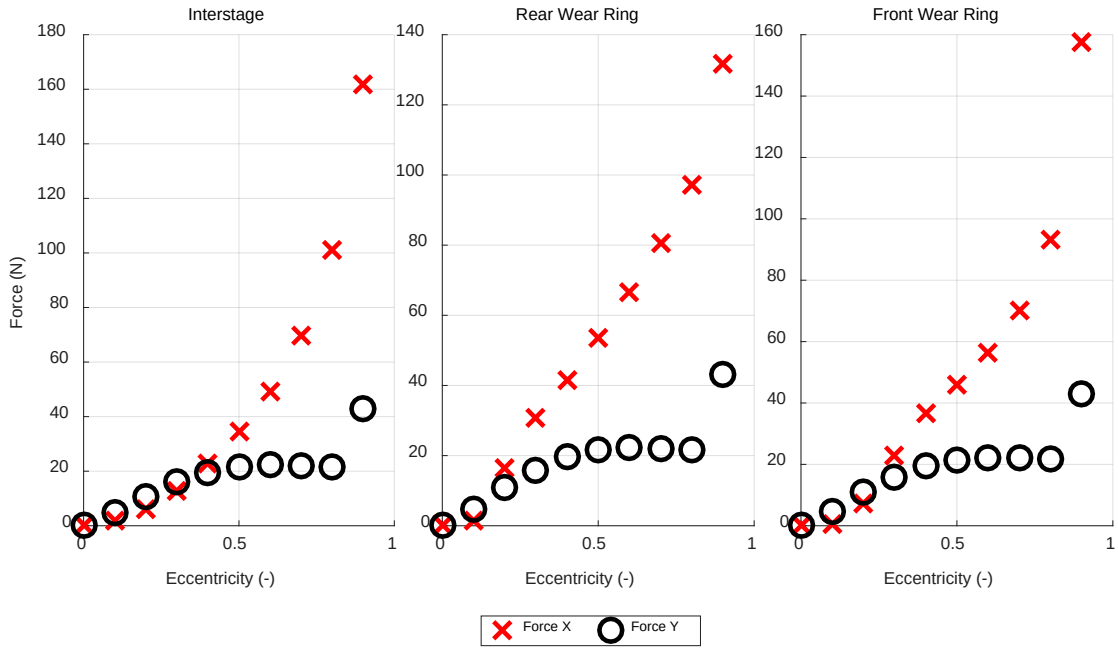

Figure D.4: Force vs. Eccentricity for seals used on 20 stage example. 1X 1cP

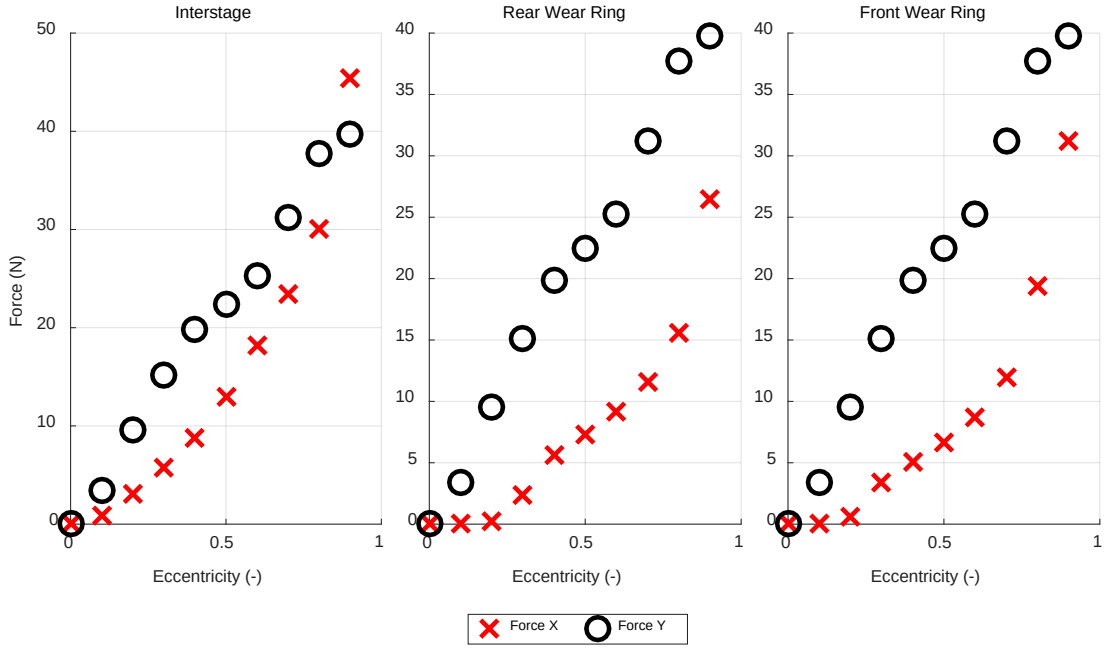

Figure D.5: Force vs. Eccentricity for seals used on 20 stage example. 3X 1cP

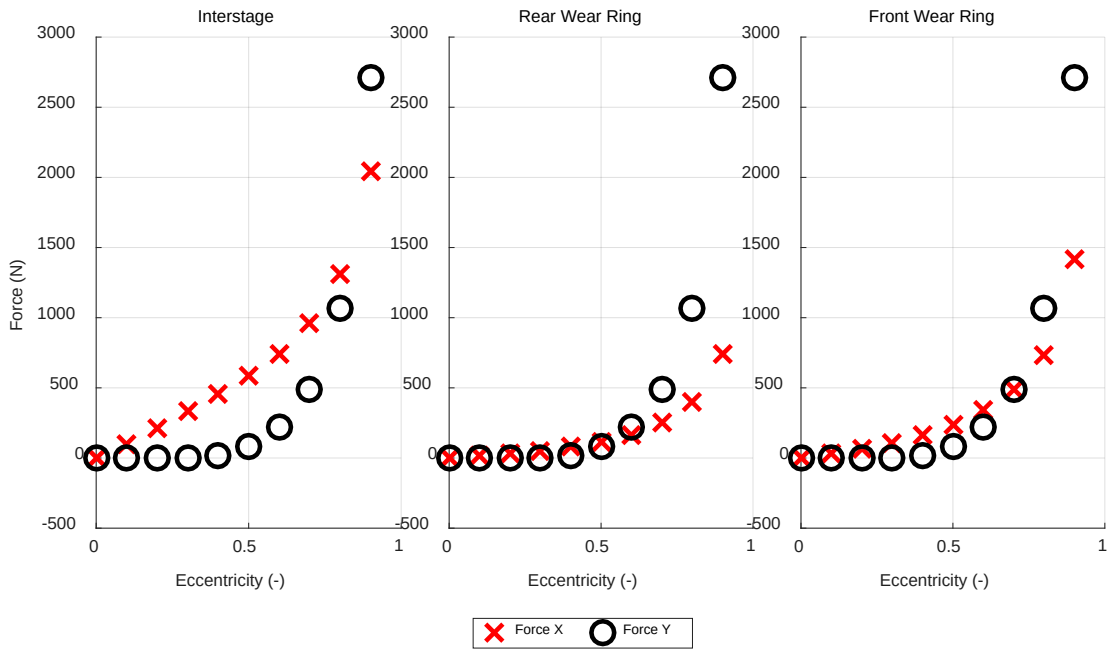

Figure D.6: Force vs. Eccentricity for seals used on 20 stage example. 1X 30cP

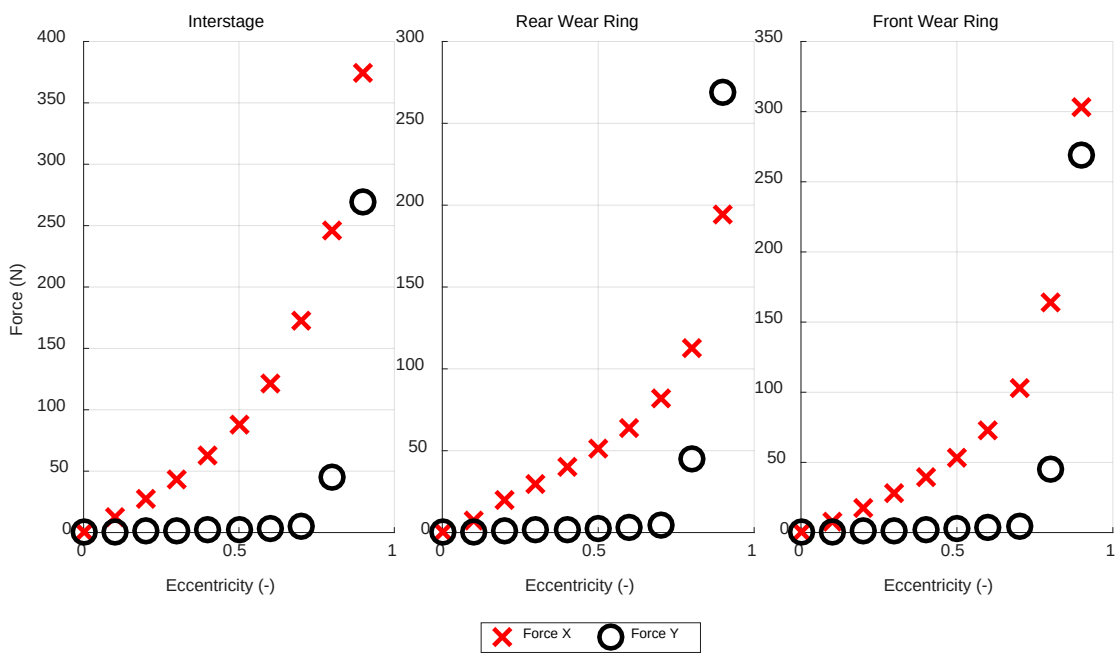

Figure D.7: Force vs. Eccentricity for seals used on 20 stage example. 3X 30cP

APPENDIX E. MAX DISPLACEMENT GRAPHS

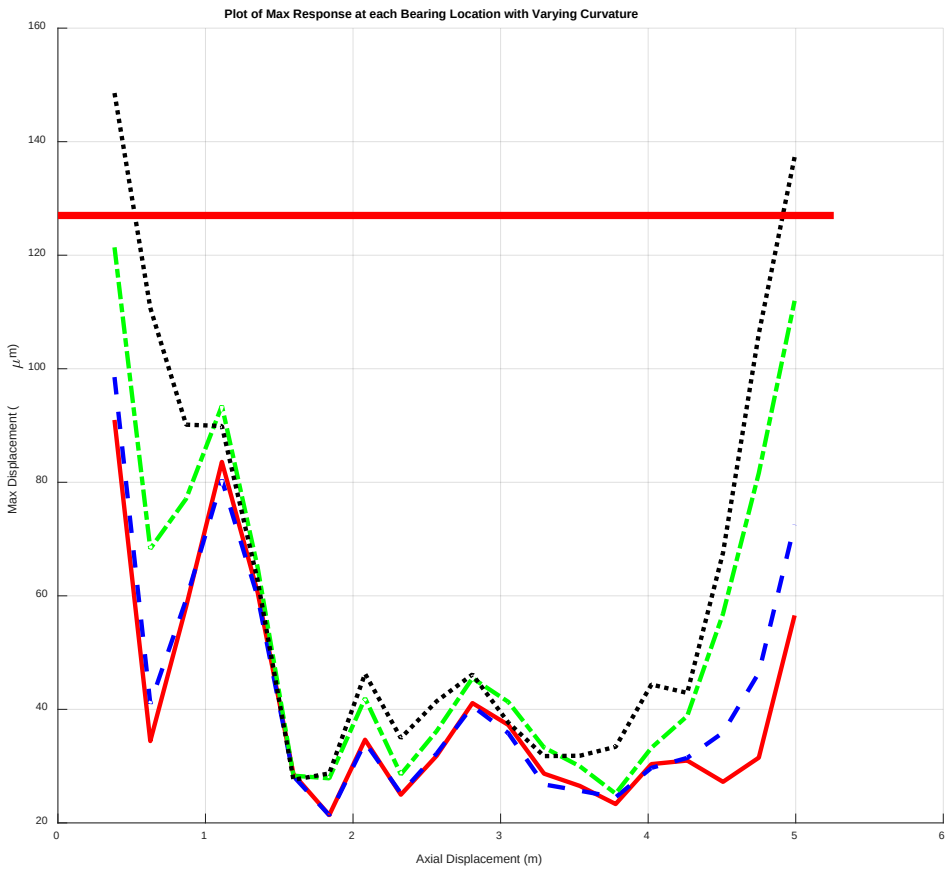

Figure E.8: Static + dynamic maximum displacement vs. axial distance for a 1X 1cP case.

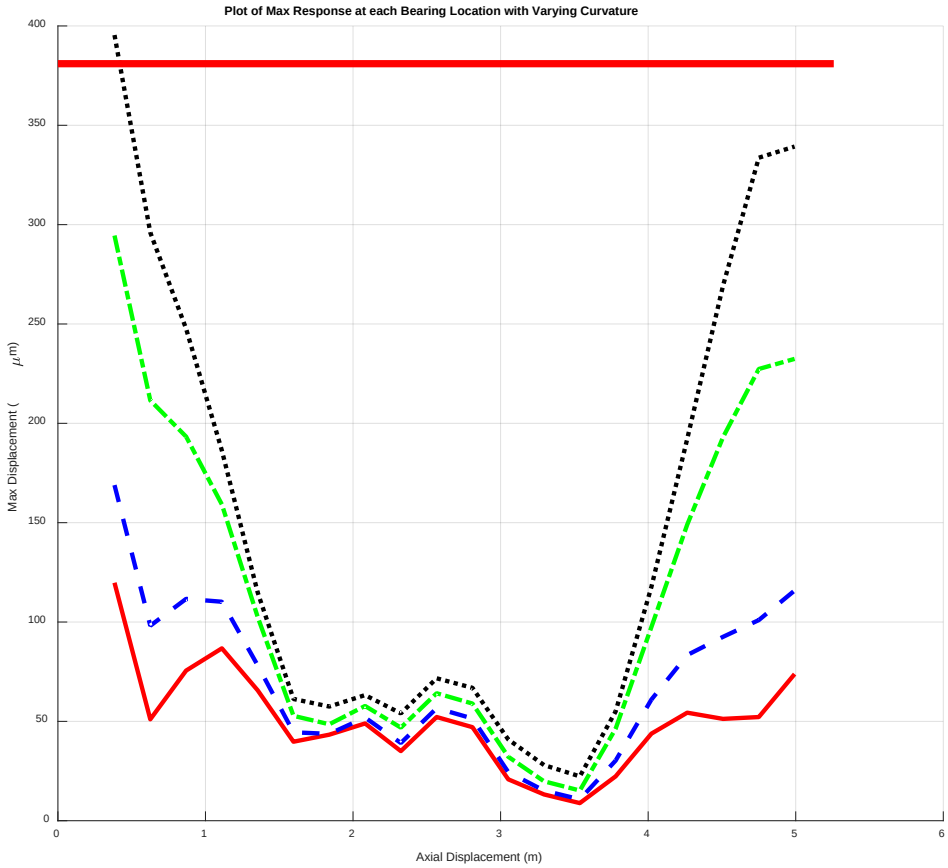

Figure E.9: Static + dynamic maximum displacement vs. axial distance for a 3X 1cP case.